

Review on “Inputs and processes affecting the distribution of particulate iron in the North Atlantic along the GEOVIDE (GEOTRACES GA01) section” by Gourain et al.

I stopped reviewing the manuscript at line 366. Due to the state of the English language, sentences are difficult, some almost impossible to understand. This needs to be fixed before the next round of review should start. I am suggesting that a native English speaking person has a look and improves the English. Sorry for that, but I need to recommend major revision. However, I am still willing to review the next version, but insist on good English grammar. Sincerely,

Christian Schlosser

Dear Dr Schlosser,

This new version of the manuscript has been proof-read by a native English speaker. Following her advices and suggestions, we modified the structure of many sentences.

You will also find our detailed answers to the specific points your raised below.

We truly hope that you will now find this manuscript suitable for publication.

Kind regards,

Arthur Gourain, on behalf of all coauthors.

Some minor points:

Line 35: Change to "...($0.21 \text{ mol mol}^{-1}$)..." [Done.](#)

Line 38ff: Include the second decimal digit for 0.7 and remove the ratio for the continental crust (you just told it 2 sentences earlier. [Done.](#)

Line 42: Maybe “suspending” would be better than “delivering”. [We modified it.](#)

Line 51: Here “deliver” would be better than “bring” [Done.](#)

Line 65ff: What do you mean with dissolution? Dissolution of inorganic PFe? Is not that also part of the regeneration? [Yes, we mean dissolution of inorganic PFe such as iron contained in basaltic grains, and this is now specified in line 67.](#)

[From our point of view, the regeneration is the recycling of biogenic PFe.](#)

Line 101: Replace “They” by “Bottles” [Done.](#)

Line 123: Rewrite sentence “before to pass”. Done.

Line 189: Remove “really” Done.

Line 190ff: What do you mean with “These authigenic particles lead to an enrichment of Mn in particle compositions.”

The elemental composition of the particles is driven by the various origins of these particles (lithogenic, biogenic, ...). For example, if the particulate bulk is dominated by lithogenic particles, its composition will have a strong imprint of lithogenic elements, e.g. Fe, Al, Ti.

Under certain conditions, manganese oxides can be generated, with the consequence of depleting dissolved manganese concentrations, and increasing the ambient particulate Mn concentrations. As this statement was indeed confusing, we reorganized the order of sentences in this section (lines 192-200).

Line 195: Replace “of direct and recent” by “for” Done

Line 226: “modal”, do you mean “mode”? Yes indeed, we changed it.

Line 242: Change “Total particulate concentrations spanned a large range of concentrations from below detection to 304 nmol L⁻¹ for PFe, 1544 nmol L⁻¹ for PAI, 3.5 nmol L⁻¹ for PMn and 402 nmol L⁻¹ for PP.” Done.

Line 275ff: include “depth” after you introduce the depth of a sample , for example “at 25 m depth” in line286. Please apply throughout the paragraph/manuscript. Done.

Line 299: Remove “candidate” Done.

Line 300: Replace “ice shelves” by “glaciers” Done.

Line 350: Remove “candidate” Done.

Figure 5: Please include in the legend what the different factors are (eg. lithogenic). Makes it easier to follow Done.

1 **Inputs and processes affecting the distribution of**
2 **particulate iron in the North Atlantic along the GEOVIDE**
3 **(GEOTRACES GA01) section**

4
5
6 Arthur Gourain^{1,2}, H  l  ne Planquette¹, Marie Cheize^{1,3}, Nolwenn Lemaitre^{1,4}, Jan-Lukas
7 Menzel Barraqueta^{5,6}, Rachel Shelley^{1,7}, Pascale Lherminier⁸ and G  raldine Sarthou¹

8
9 1-UMR 6539/LEMAR/IUEM, CNRS, UBO, IRD, Ifremer, Technop  le Brest Iroise, Place Nicolas Copernic,
10 29280 Plouzan  , France

11 2- now at Ocean Sciences Department, School of Environmental Sciences, University of Liverpool, Liverpool,
12 L69 3GP, United Kingdom

13 3- now at Ifremer, Centre de Brest, G  osciences Marines, Laboratoire des Cycles G  ochimiques (LCG), 29280
14 Plouzan  , France

15 4- now at Department of Earth Sciences, Institute of Geochemistry and Petrology, ETH-Z  rich, Z  rich,
16 Switzerland

17 5- GEOMAR, Helmholtz Centre for Ocean Research Kiel, Wischhofstra  e 1-3, 24148 Kiel, Germany

18 6- now at Department of Earth Sciences, Stellenbosch University, Stellenbosch, 7600, South Africa

19 7- now at Earth, Ocean and Atmospheric Science, Florida State University, Tallahassee, Florida, 32310, USA

20 8- Ifremer, Univ. Brest, CNRS, IRD, Laboratoire d'Oc  anographie Physique et Spatiale (LOPS), IUEM, F-
21 29280, Plouzan  , France

22
23 *Correspondence to: helene.planquette@univ-brest.fr*

24
25 **Abstract**

26 The [aim of the](#) GEOVIDE cruise (May-June 2014, R/V *Pourquoi Pas?*) ~~aimed-was~~ to provide a better
27 understanding ~~on-of~~ trace metal biogeochemical cycles in the North Atlantic [Ocean](#). As [marine](#) particles play a
28 key role in the global biogeochemical cycle of trace elements in the ocean, we discuss the distribution of
29 particulate iron (PFe), in [light-relation to the distribution of](#) particulate aluminium (PAI), manganese (PMn) and
30 phosphorus (PP) ~~distributions~~. Overall, 32 full vertical profiles were collected for trace metal analyses,
31 representing more than 500 samples. This resolution provides a solid basis for assessing concentration
32 distributions, elemental ratios, size-fractionation, [and/or](#) adsorptive scavenging processes in key areas of the
33 thermohaline circulation. Total particulate iron (~~PFe~~)-concentrations ranged from as low as 9 pmol L⁻¹ in surface
34 [waters of the](#) Labrador Sea ~~waters~~ to 304 nmol L⁻¹ near the Iberian margin, while median PFe concentrations of
35 1.15 nmol L⁻¹ were measured over the sub-euphotic ocean interior.

36 Within the Iberian Abyssal Plain, [the](#) ratio of PFe ~~over-to~~ [particulate-aluminium](#) (PAI) ~~was~~ identical to the
37 continental crust [molar](#) ratio (0.21), indicating the important influence of crustal particles in the water column.

38 Overall, the lithogenic component explained more than 87% of PFe variance along the section. Within the
39 Irminger and Labrador basins, the formation of biogenic particles led to an increase of the PFe/PAI ratio (up to
40 0.7 mol mol⁻¹) compared to the continental crust ratio (0.21 mol mol⁻¹). Continental margins provide important
41 high quantities of particulate trace elements (up to 10 nmol L⁻¹ of PFe) to the open ocean, and in the case of the
42 Iberian or example margin, horizontal advection of PFe was visible more than 250km away from the Iberian
43 margin. Additionally, several benthic nepheloid layers were observed more than 200 m
44 above the seafloor were encountered along the transect, especially in the Icelandic, Irminger and Labrador basins,
45 delivering particles with high PFe content of up to 89 nmol L⁻¹.

46 1. Introduction

47 Particles play a key role in the ocean where they drive the residence time of most elements (Jeandel and Oelkers,
48 2015), and strongly influence the global biogeochemistry of macro- and micro-nutrients including iron (Milne et
49 al., 2017). In the surface ocean, biological activity produces biogenic suspended matter through planktonic
50 organisms, while atmospheric deposition (Baker et al., 2013; Jickells et al., 2005), riverine discharge (Aguilar-
51 Islas et al., 2013; Berger et al., 2008; Ussher et al., 2004) or ice-melting (Hawkings et al., 2014; Lannuzel et al.,
52 2011, 2014) bring mostly lithogenic derived particles to surface waters. These particulate inputs are highly
53 variable, both spatially and seasonally, around in the world's oceans. At depth, benthic and shelf sediment
54 resuspension (e.g. Aguilar-Islas et al., 2013; Cullen et al., 2009; Elrod et al., 2004; Fitzwater et al., 2000; Hwang
55 et al., 2010; Lam et al., 2015; Lam and Bishop, 2008; McCave and Hall, 2002), and hydrothermal activity
56 (Elderfield and Schultz, 1996; Lam et al., 2012; Tagliabue et al., 2010, 2017; Trefry et al., 1985), provides
57 important amounts of particles to the water column. Moreover, authigenic particles can be produced *in-situ* by
58 aggregation of colloids (Bergquist et al., 2007) or oxidation processes (Bishop and Fleisher, 1987; Collier and
59 Edmond, 1984). Thus, oceanic particles result from a complex combination of these different sources and
60 processes (Lam et al., 2015).

61 Particles represent the main part of the total iron pool in the upper water column, the total iron pool in the upper water column is
62 dominated by marine particles (Radic et al., 2011) which and strongly interact with the dissolved pool (e.g.
63 Ellwood et al., 2014). Indeed, dissolved iron can be scavenged onto particles (Gerringa et al., 2015; Rijkenberg et
64 al., 2014), incorporated into biogenic particles (Berger et al., 2008) or produced by remineralisation of particles
65 (Dehairs et al., 2008; Sarthou et al., 2008). Interestingly, the concept of "reversible scavenging" (i.e. release at
66 depth of dissolved iron previously scavenged onto particles) has been advocated recently (Dutay et al., 2015;
67 Jeandel and Oelkers, 2015; Labatut et al., 2014), while other studies reveal distinct dissolution processes (e.g.
68 Oelkers et al., 2012; Cheize et al., 2018). Slow dissolution of particulate iron at margins has also been evoked as
69 a continuous fertilizer of primary production and should be considered as a source of dissolved iron (e.g. Jeandel
70 et al., 2011; Jeandel and Oelkers, 2015; Lam and Bishop, 2008). Within or below the mixed layer, the rates of
71 regeneration processes can also impact the bioavailable pool of iron, among other trace metals (e.g. Ellwood et
72 al., 2014; Nuester et al., 2014). However, the rates of these processes are not yet fully constrained. The study of
73 particulate iron is thus essential to better constrain its marine biogeochemical cycle. Interest has grown in this
74 subject, received a growing interest over the last 10 years, in particular (e.g. Bishop and Biscaye, 1982; Collier
75 and Edmond, 1984; Frew et al., 2006; Lam et al., 2012; Milne et al., 2017; Planquette et al., 2011, 2013; Sherrell
76 et al., 1998) and, to our knowledge, only two studies have been performed at an ocean-wide scale and published
77

78 ~~so far~~: the GA03 GEOTRACES North Atlantic Zonal Transect (Lam et al., 2015; Ohnemus and Lam, 2015) and
79 the GP16 GEOTRACES Pacific Transect (Lam et al., 2017; Lee et al., 2017).

80 ~~In this~~ Within this global context, this paper presents the particulate iron distribution ~~in-of~~ the North Atlantic
81 Ocean, along the GEOTRACES GA01 section (GEOVIDE), and discusses the various sources and processes
82 affecting ~~its-particulate iron~~ distribution, using particulate aluminium, phosphorus or manganese ~~distributions to~~
83 ~~support our conclusions~~.

85 2. Methods

86 2.1. Study area

87 Particulate samples were collected at 32 stations during the GEOVIDE (GEOTRACES GA01 section) cruise
88 between May and June 2014 aboard the R/V *Pourquoi Pas?* in the North Atlantic Ocean (Sarhou et al., 2018).
89 The sampling spanned several biogeochemical provinces (Figure 1), ~~starting over that first comprised~~ the Iberian
90 margin (IM, Stations 2, ~~44~~ and ~~14~~), ~~and proceeding to~~ the Iberian Abyssal Plain (IAP, Stations 11 to 17), the
91 Western European Basin (WEB, Station 19 to Station 29) and the Icelandic Basin (IcB, Stations 32 to 36). Then,
92 samples were collected above the Reykjanes Ridge (RR, Station 38), in the Irminger Basin (IrB, Stations 40 to
93 60), close to the Greenland shelf (GS, Stations 53, ~~56~~ and 61), the Labrador Basin (LB, Stations 63 to 77) and
94 finally close the Newfoundland shelf (NS, Station 78) (Figure 1). The North Atlantic is characterized by a complex
95 circulation (briefly described in section ~~23.1~~ and in detail by Zunino et al. (2017) and García-Ibáñez et al. (2015),
96 and is one of the most productive regions of the global ocean (Martin et al., 1993; Sanders et al., 2014), with a
97 complex phytoplankton community structure composed of diverse taxa (Tonnard et al., in prep.).

100 2.2. Sampling

101 Samples were collected using the French GEOTRACES clean rosette, equipped with twenty-two 12 L GO-FLO
102 bottles (two bottles were leaking and were ~~never-not~~ deployed during the cruise). GO-FLO bottles (General
103 Oceanics) were initially cleaned in the home laboratory (LEMAR) following the GEOTRACES procedures
104 (Cutter and Bruland, 2012). The rosette was deployed on a 14 mm Kevlar cable with a dedicated, custom-designed
105 clean winch. Immediately after recovery, the GO-FLO bottles were individually covered at each end with plastic
106 bags to minimize contamination. They were then transferred into a clean container (class-100) for sampling, ~~and~~
107 ~~the filters processed under a laminar flow unit~~. On each cast, nutrient and/or salinity samples were taken to check
108 potential leakage of the GO-FLO bottles.

109 Filters were cleaned following the GEOTRACES protocols (<http://www.geotraces.org/images/Cookbook.pdf>)
110 and kept in acid-cleaned 1 L LDPE bottles (Nalgene) filled with ultrapure water (Milli-Q, resistivity of 18.2 MΩ
111 cm) until use. All filters were 25 mm diameter in order to optimize ~~the~~ signal over the filter blank, except at the
112 surface depth where 47 mm diameter filters ~~were used~~. ~~The filters were~~ mounted on acid-cleaned polysulfone
113 filter holders (NalgeneTM) ~~were used~~. Prior to filtration, the GO-FLO bottles were shaken three times, as
114 recommended in the GEOTRACES cookbook to avoid settling of particles in the lower part of the bottle. GO-
115 FLO bottles were pressurized to < 8 psi with 0.2 μm filtered ~~nitrogen gas~~ (N₂, Air Liquide). Seawater was then
116 filtered directly through paired filters (Pall Gelman SuporTM 0.45 μm polyetersulfone, and Millipore mixed ester

Formatted: Font: (Default) Times New Roman

Formatted: Font: (Default) Times New Roman

117 cellulose MF 5 μm) mounted in Swinnex polypropylene filter holders (Millipore), following Planquette and
118 Sherrell (2012) inside the clean container. Filtration was operated until the bottle was empty or until the filter
119 clogged; the volume filtered ranged from 2 L for surface samples to 11 L within the water column. After
120 filtration, filter holders were disconnected from the GO-FLO bottles and a gentle vacuum was applied using a
121 syringe in order to remove any residual water under a laminar flow hood. Filters were then removed from the filter
122 holders with plastic tweezers ~~that~~ (which were rinsed with Milli-Q between samples). Most of the remaining
123 seawater was removed via 'sipping' by capillary action, when placing the non-sampled side of the filter onto a
124 clean 47 mm supor filter. ~~E~~Then, each filter pair was then placed in an acid-cleaned polystyrene PetriSlide[®]
125 (Millipore), double bagged, and finally stored at -20°C until analysis at LEMAR. Between casts, filter holders
126 were thoroughly rinsed with Milli-Q, placed in an acid bath (5% Trace metal grade HCl) for 24 hours, then rinsed
127 with Milli-Q.

128 At each station, process blanks were collected as follows: 2 L of a deep (1000 m) and a shallow (40 m) seawater
129 samples were first filtered through a 0.2 μm pore size capsule filter (Pall Gelman Acropak 200) mounted on to the
130 outlet of the GO-FLO bottle before ~~te~~ passing through the particle sampling filter, which was attached directly to
131 the swinnex filter holder.

132

133

2.3. Analytical methods

134 ~~I~~Back in the home laboratory, sample handling was performed inside a clean room (Class 100). All solutions were
135 prepared using ultrapure water (Milli-Q) and all plasticware had been acid-cleaned before use. Frozen filters,
136 collected within the mixed layer ~~depth~~ or within nepheloid layers, were first cut in half using a ceramic blade: one
137 filter half was dedicated to total digestion (see below), while the other half was archived at -20°C for SEM analyses
138 or acid leaching of "labile" metals (Berger et al., 2008; to be published separately).

139 Filters were digested following the method described in Planquette and Sherrell (2012). Filters were placed on the
140 inner wall of acid-clean 15 mL PFA vials (SavillexTM), and 2 mL of a solution containing 2.9 mol L⁻¹ hydrofluoric
141 acid (HF, suprapur grade, Merck) and 8 mol L⁻¹ nitric acid (HNO₃, Ultrapur grade, Merck) was added to each vial.
142 Vials were then closed and refluxed at 130°C on a hot plate for 4 hours, after which the ~~and~~ filters were removed.

143 After cooling, the digest solution was evaporated at 110°C ~~until~~ to near dryness. Then, 400 μL of concentrated
144 HNO₃ (Ultrapur grade, Merck) was added, and the solution was re-evaporated at 110°C. Finally, the obtained
145 residue was dissolved with 3 mL of a 0.8 mol L⁻¹ HNO₃ (Ultrapure grade, Merck). This archived solution was
146 transferred to an acid cleaned 15 mL polypropylene centrifuge tube (Corning[®]) and stored at 4°C until analyses.

147 All analyses were performed on a sector field inductively coupled plasma mass spectrometer (SF-ICP-MS
148 Element 2, Thermo-Fisher Scientific). Samples were diluted by a factor of 7 on the day of analysis in acid-washed
149 13 mm (outer diameter) rounded bottom, polypropylene centrifuge tubes (VWR) with 0.8 mol L⁻¹ HNO₃ (Ultrapur
150 grade, Merck) spiked with 1 $\mu\text{g L}^{-1}$ of Indium (¹¹⁵In) solution in order to monitor the instrument drift. Samples
151 were introduced with a PFA-ST nebulizer connected to a quartz cyclonic spray chamber (Elemental Scientific

152 Incorporated, Omaha, NE) via a modified SC-Fast introduction system consisting of an SC-2 autosampler, a six-
153 port valve and a vacuum-rinsing pump. The autosampler was contained under a HEPA filtered unit (Elemental
154 Scientific). Two 6-points, matrix-matched multi-element standard curves with concentrations bracketing the range
155 of the samples were run at the beginning, the middle and the end of each analytical run. Analytical replicates were
156 made every 10 samples, while accuracy was determined by performing digestions of the certified reference

157 material BCR-414 (plankton, Community Bureau of Reference, Commission of the European Communities),
158 PACS-3 and MESS-4 (marine sediments, National Research Council Canada), following the same protocol as
159 used for the samples. Recoveries were typically within 10% of the certified values (and within the error of the
160 data, taken from replicate measurements, Table 1). Once all data were normalized to an ¹¹⁵In internal standard and
161 quantified using an external standard curve, the dilution factor of the total digestion was accounted for. Obtained
162 The elemental concentrations were obtained per filter (pmol/filter) and were then corrected by the process blank-
163 correcteds described above. Finally, pmol/filter values were divided by the volume of water filtered through the
164 stacked filters.

165 Total concentrations (sum of small size fraction (0.45-5 µm) and large (>5 µm) size fraction) of particulate trace
166 elements are reported in Table S1 (supplementary data).

167
168

2.4. Ancillary data:

169 ~~Potential temperature (θ), salinity (S), and transmissometry data were retrieved from the CTD sensors (CTD~~
170 ~~SBE911 equipped with a SBE42).~~

171
172

2.5.4. Positive matrix factorisation

173 Positive Matrix Factorisation (PMF) was run to characterise the main factors influencing the particulate trace
174 elements variances along the GEOVIDE section. In addition to PFe, PAI, PMn, and PP, nine additional elements
175 were included in the PMF: Y, Ba, Pb, Th, Ti, V, Co, Cu and Zn. The analysis-PMF whas been conducted on
176 samples where all the 13 elements previously cited were above their detection limits; after selection, 445 of the
177 549 existing data points were used. Analyses were performed using the PMF software, EPA PMF 5.0, developed
178 by the USA Environmental Protection Agency (EPA). Three to six factor mModels have been tested with were
179 run on the data, several factors number (from 3 to 6) T, after full error estimation of each model, we decide to use
180 the configuration that provideding the lowest errors estimation and in consequence the (i.e. was the most reliable)
181 was the-

182 In consequence, models were set up with four factor model. To ensure stability this model was and were run 100
183 times to observe the stability of the obtained results. After displacement, error estimations and bootstraps error
184 estimations, the model was recognised as stable.

185
186

2.6.5. Derived and ancillary parameters

187 To investigate The PFe/PAI ratio can be used to estimate the proportion of lithogenic particles iron within the bulk
188 particulate fraetiiron, we used. A comparison with the Upper Continental Crust (UCC) Fe/Al molar ratio (0.21)
189 of Taylor and McLennan (1995) s, 0.21, was used to calculate the lithogenic components of particles (%PFe_{litho})
190 following Eq. (1):

191
192

$$\%PFe_{litho} = 100 * \left(\frac{PAI}{PFe} \right)_{sample} * \left(\frac{PFe}{PAI} \right)_{UCC} \text{ ratio} \quad (1)$$

193
194

Then the non-lithogenic PFe is simply obtained using Eq. (2):

195
196
$$\%PFe_{\text{non-litho}} = 100 - \%PFe_{\text{litho}} \quad (2)$$

197

198 Note that while (Both the lithogenic and non-lithogenic fraction of PFe are estimated using the UCC ratio. Spatial
199 and temporal variation of the lithogenic components ratio may falsely influence the estimated fraction value. The
200 %PFe_{litho} and %PFe_{non-litho} proxies are interesting tools to evaluate the importance of lithogenic and non-lithogenic
201 (either biogenic or authigenic), but they have to be used carefully, as the spatial and temporal variation of the
202 lithogenic component ratios may falsely influence the estimated fraction value.

203
204 In addition to PAI, PMn can be used as a tracer of inputs from shelf resuspension (Lam and Bishop, 2008). Indeed,
205 Mn is really sensitive to bacteria-mediated oxidation mediated by bacteria (Tebo et al., 1984; Tebo and Emerson,
206 1985) and forms manganese oxides (MnO₂). These authigenic particles lead to an enrichment of Mn in particles
207 compositions. In order to track the influence of shelf resuspension, a percentage of sedimentary inputs “%bulk
208 sediment inputs” can be estimated using the PMn/PAI ratio from the GEOVIDE samples and the PMn/PAI UCC
209 value (0.0034; Taylor and McLennan, 1995) according to the following equation:

210
$$\% \text{bulk sediment PMn} = 100 * \left(\frac{\text{PAI}}{\text{PMn}} \right)_{\text{sample}} * \left(\frac{\text{PMn}}{\text{PAI}} \right)_{\text{UCC ratio}} \quad (3)$$

211 This proxy is can be a good indicator of direct and recent sediment resuspension. We assume that particles newly
212 resuspended in the water column will have the same PMn/PAI ratio than as the UCC ratio, leading to a “%bulk
213 sediment Mn” of 100%. This value will decrease by authigenic formation of Mn oxides. This proxy assumes
214 homogeneity of the sediment PMn/PAI ratio throughout the GEOVIDE section. However, which this is may be
215 not be completely the case at every station. In consequence, this proxy is should only a tool be used to identify new
216 benthic resuspension at specific locations; and inter-comparison between several locations is not possible may not
217 be appropriate. When a sample presents a “%bulk sediment Mn” greater than 100%, we have assigned a maximum
218 value of 100% to simplify the following discussion. As the Mn cycle can also be affected influenced by biotic biologic
219 uptake (e.g. Peers and Price, 2004; Sunda and Huntsman, 1983), this proxy is only used at depths where biologic
220 activity was negligible (i.e. below 150m depth).

221 Potential temperature ($\theta^\circ\theta$), salinity (S), and transmissometry data were retrieved from the CTD sensors (CTD
222 SBE911 equipped with a SBE43).

223 224 225 **3. Results**

226 *3.1. Hydrography and biological setting*

227 Here, we briefly describe the hydrography encountered during the GEOVIDE section (Figure 2); as a thorough
228 description is available in García-Ibáñez et al. (2015). In the beginning At the start of the section-, the warm and
229 salty Mediterranean Water (MW, S=36.50, $\theta^\circ=11.7^\circ\text{C}$) was sampled between 600 and 1700 m in the Iberian
230 Abyssal Plain (IAP). MW resulted from the mixing between the Mediterranean Overflow Water plume coming
231 from the Mediterranean Sea and local waters. Surface water above the Iberian Shelf was characterised by low

Formatted: Font: Italic

232 salinity ($S=34.95$) at station 2 and 4 compared to surrounding water masses. Close to the floor of the Iberian
233 Abyssal Basin, the North East Atlantic Deep Water (NEADW, $S=34.89$, $\theta=2.0^{\circ}\text{C}$) spread ~~south~~northward. The
234 North Atlantic Central Water (NACW, $S>35.60$, $\theta>12.3^{\circ}\text{C}$) was the warmest water mass of the transect and was
235 observed in the subsurface layer of the Western European Basin and Iberian Abyssal Plain. An old Labrador Sea
236 Water (LSW, $S=34.87$, $\theta=3.0^{\circ}\text{C}$) flowed inside the Western European and Icelandic Basins, between 1000 and
237 2500m depth.
238 -In the Icelandic Basin, below the old LSW, the Iceland-Scotland Overflow Water (ISOW, $S=34.98$, $\theta=2.6^{\circ}\text{C}$)
239 spread along the Reykjanes Ridge slope. This cold water, originating from the Arctic, led to the formation of
240 NEADW after mixing with surrounding waters. North Atlantic hydrography was impacted by the northward
241 flowing of the North Atlantic Current (NAC), which carried ~~up~~-warm and salty waters from the subtropical area.
242 ~~By~~Due to air-sea interactions and mixing with surrounding water, the NACW is cooled ~~down~~ and freshened in
243 the subpolar gyre and is transformed in Subpolar Mode Water (SPMW). ~~When NAC crossed the Mid-Atlantic~~
244 ~~ridge through the Charlie Gibbs Fracture Zone (CGFZ), it created the Subpolar Mode Water (SPMW).~~ The
245 ~~recirculation-formation~~ of SPMW inside the Icelandic and Irminger Basins ~~leads~~ to the formation of regional
246 modal waters: the Iceland Subpolar Mode Water (IcSPMW, $S=35.2$, $\theta=8.0^{\circ}\text{C}$) and the Irminger Subpolar Mode
247 Water (IrSPMW, $S=35.01$, $\theta=5.0^{\circ}\text{C}$), respectively. IcSPMW was a relatively warm water mass with potential
248 temperature up to 7°C (García-Ibáñez et al., 2015). Another branch of the NAC mixed with Labrador Current
249 waters to form the relatively fresh SubArctic Intermediate Water (SAIW, $S<34.8$, $4.5^{\circ}\text{C}<\theta<6^{\circ}\text{C}$).
250 The Irminger Basin is a complex area with a multitude of water masses. In the middle of the basin, an old LSW,
251 formed one year before (Straneo et al., 2003), spread between 500 and 1200 m depth. Close to the bottom, the
252 Denmark Strait Overflow Water (DSOW, $S=34.91$) flowed across the basin. Greenland coastal waters were
253 characterised by low salinity values, down to $S=33$. The strong East Greenland Current (EGC) flowed southward
254 along the Greenland shelf in the Irminger Basin. ~~When reaching~~At the southern tip of Greenland, this current
255 entered the Labrador Basin along the west coast of Greenland and followed the ~~outskirts~~-outline of the basin until
256 the Newfoundland shelf. In the Labrador Basin, the deep convection of SPMW at 2000 m was involved in the
257 formation of the LSW ($S=34.9$, $\theta=3.0^{\circ}\text{C}$) (García-Ibáñez et al., 2015; Yashayaev and Loder, 2009). Above the
258 Newfoundland Shelf, surface waters were affected by discharge from rivers and ice-melting and characterised by
259 extremely low salinity for open ocean waters, below 32 in the first 15 meters.

260 3.2. Section overview

261 Total particulate iron (~~PFe~~), aluminium (~~PAI~~), manganese (~~PMn~~) and phosphorus (~~PP~~) concentrations spanned a
262 large range of concentrations from below detection to 304, 1544, -3.5 and 402 nmol L^{-1} respectively. ~~The ranges~~
263 ~~of concentrations are comparable to other studies recently published (Table 2).~~
264 PFe, PAI, and PMn were predominantly found (>90%) in particles larger than $5\ \mu\text{m}$, except in surface waters,
265 where $9 \pm 8.6\%$ of PFe, ~~38.8 \pm 8.6 % of PP~~, $10.9 \pm 15.4\%$ of PAI and $32.8 \pm 16.6\%$ of PMn, ~~38.8 \pm 8.6 % of~~
266 ~~PP~~ were hosted by smaller particles ($0.45\text{-}5\ \mu\text{m}$). ~~The ranges of concentrations are comparable to other studies~~
267 ~~recently published (Table 2).~~ Data are shown in Figure 3.

268

269 *3.3. Open Ocean stations: stations from the Iberian Abyssal Plain (stations 11 to 17), Western*
270 *European Basin (stations 19 to 29), Icelandic Basin (stations 32 to 36), Reykjanes Ridge (station 38),*
271 *Irminger Basin (stations 40 to 60; except Stations 53 and 56) and to the Labrador Basin (stations 63 to*
272 *77, except stations 53, 56 and 61)*

273 This concerns all stations ~~between from~~ station 11 to 77, with the exception of stations 53, 56 and 61 ~~that which~~
274 ~~were sampled close to the Greenland and Newfoundland coast (Figure 1), respectively.~~

275 Particulate iron concentration vertical profiles ~~presented showed~~ identical patterns at all of the open ocean stations
276 ~~sampled in each oceanic basin~~ encountered along the section. Median PFe was ~~as~~ low at 0.25 nmol L⁻¹ within the
277 first 100 m and steadily increased with depth. However, at two stations, elevated concentrations were determined
278 in the upper 100 m, up to 4.4 nmol L⁻¹ at station 77 at 40 m and 7 nmol L⁻¹ at station 63 between 70 and 100 m
279 depth. PFe concentrations gradually increased with depth, with a median PFe of 1.74 nmol L⁻¹ below 1000m.
280 Close to the seafloor of some stations (26, 29, 32, 34, 49, 60, and 71), high concentrations of PFe were observed,
281 up to 88 nmol L⁻¹ (station 71 at 3736 m). These high PFe values were associated with low beam transmissometry
282 values ~~≤ inferior or equal to~~ 97.7%, (Figure 9b and supplementary table S2).

283 Particulate aluminium (PAI) and manganese (PMn) profiles were similar to PFe profiles, with low concentrations
284 measured in the first 100 m (1.88 nmol L⁻¹ and 55 pmol L⁻¹, respectively) ~~and which~~ increased towards the
285 seafloor. Close to the seafloor, high concentrations were determined at the same stations cited above for PFe, with
286 a maximum of 264 nmol L⁻¹ and 3.5 nmol L⁻¹ for PAI and PMn respectively at station 71 (supplementary Table
287 S1). Highest particulate phosphorus (PP) concentrations were in the ~~first uppermost~~ 50 m, with a median value of
288 66 nmol L⁻¹. Deeper in the water column, below 200 m, PP concentrations decreased to values below 10 nmol L⁻¹.
289 Inter-basins differences were observed within the surface samples, with median PP concentration being higher
290 in the Irminger Basin (127 nmol L⁻¹) than in the Iberian Abyssal Plain (28 nmol L⁻¹) (Figure 3).

291 Finally, above the Reykjanes Ridge, PP, PMn, PAI and PFe concentrations were in the same range ~~than as~~ the
292 surrounding open ocean stations. However, close to the seafloor, high concentrations were measured, with PFe,
293 PAI, and PMn reaching 16.2 nmol L⁻¹, 28.8 nmol L⁻¹, and 0.51 nmol L⁻¹ at 1354 m, respectively (Figure 3 and
294 ~~supplementary material~~ Table S1).

295
296 *3.4. Margins and Shelves: Iberian Margin (stations 1 to 4), Greenland coast (stations 53, 56*
297 *and 61) and Newfoundland Shelf (station 78)*

298
299 The Iberian margin was characterised by low beam transmissometry values at station 2 (88% at 140 m, Figure
300 49b) suggesting significant particle concentrations. Particulate iron concentrations varied ~~between from~~ 0.02 nmol
301 L⁻¹ to 304 nmol L⁻¹. Within the first 50 m, PFe concentrations decreased towards the shelf break where PFe
302 dropped ~~down~~ from 2.53 nmol L⁻¹ (station 2) to 0.8 nmol L⁻¹ (Station 1). ~~At all three stations,~~ PFe concentrations
303 increased with depth ~~at all three stations~~ and reached a maximum ~~at the be~~ close to the seafloor. ~~As an~~ For
304 ~~example,~~ 300 nmol L⁻¹ of PFe was ~~measured~~ determined at 138.5 m ~~at tom~~ of station 2 (138.5 m) with more than
305 300 nmol L⁻¹ of PFe. Lithogenic tracers, such as PAI or PMn, presented similar profiles to PFe with concentrations
306 ranging ~~between from~~ 0.11 and 1544 nmol L⁻¹, and from below detection limit to 2.51 nmol L⁻¹ respectively
307 (Figure 3, ~~supplementary material~~ Table S1). Total particulate phosphorus (PP) concentrations were relatively

Formatted: Superscript

low in the surface ranging from undetectable values below detection to 38 nmol L⁻¹; concentrations decreased with depth and were less than 0.7 nmol L⁻¹ below 1000 m depth.

In the vicinity of the Greenland shelf, PFe concentrations had a high median value of 10.8 nmol L⁻¹ and were associated with high median PAI and PMn concentrations of 32.3 nmol L⁻¹ and 0.44 nmol L⁻¹, respectively. Concentrations of PP were high at the surface with a value of 197 nmol L⁻¹ at 25 m of station 61. Then, PP concentrations decreased strongly, to less than 30 nmol L⁻¹, below 100 meters depth. Furthermore, beam transmissometry values in surface waters at these three stations, were the lowest of the entire section, with values below 85-%.

Close to the Newfoundland margin, surface waters displayed a small load of particulate trace metals as PFe, PAI, and PMn were below 0.8 nmol L⁻¹, 2 nmol L⁻¹, and 0.15 nmol L⁻¹, respectively. Then, close to the bottom of station 78, at 371 m, beam transmissometry values dropped to 94% and were associated with extremely high concentrations of PFe=168 nmol L⁻¹, PAI=559 nmol L⁻¹, and PMn=2 nmol L⁻¹. Total PP concentrations in the first 50 m ranged from 35 to 97 nmol L⁻¹. Below 50 m the surface, PP remained relatively high with values up to 16 nmol L⁻¹ throughout the water column. (Figure 3 and supplementary-material-Table S1).

4. Discussion

Our goal in this work was to investigate mechanisms that drive the distribution of PFe in the North Atlantic, in particular the different routes of supply and removal. Possible candidate sources of PFe include lateral advection offshore from margins, atmospheric inputs, continental run-off, melting ice shelves and icebergs, resuspended sediments, hydrothermal inputs and biological uptake. Removal processes include remineralization, and dissolution processes and sediment burial.

In the following sections, we examine each of these sources and processes, explore the evidence for their relative importance, and use compositional data to estimate the particle types and host phases for iron and associated elements.

4.1. Analysis of the principal factors controlling variance: near-ubiquitous influence of crustal particles in the water column

The positive matrix factorisation analysis (Figure 5) has been realised was undertaken on the entire dataset, in consequence, the factors described below are highly influenced by the major variations of particulate element concentrations (usually at the interfaces, i.e. margin, seafloor, surface layer). The positive matrix factorisation, shown in Figure 5, indicate factorisation, shown in Figure 5, indicates the overall variances explained by each of the 45 factors. The first factor is characterised by lithogenic elements, representing 86.8% of the variance of PFe, 75.8% of PAI and 90.5% of PTi. The second factor is correlated with both Mn and Pb and explains no less than 76.5% and 77.0% of their respective variances. Ohnemus and Lam (2015) observed this co-relation between manganese and lead particles and explained it by the co-transport on Mn-oxides (Boyle et al., 2005). The formation of barite is causing explains the third factor, and constraineding 87.7% of the Ba variance in the studied regions. Biogenic barite accumulation within the mesopelagic layer is related to bacterial activity and organic remineralisation of biogenic material (Lemaitre et al., 2018a). A biogenic component is the fourth factor and explained most of particulate phosphorus PP variance, 83.7%. The micronutrient trace metals, copper, cobalt and zinc, had more than a quarter of their variances influenced by this factor. Note that tThe biogenic contribution to

347 [PFeparticulate iron](#) and other [particulate](#) trace elements will be discussed in another paper (Planquette et al., in
348 [prep](#)).

349 These results indicate that along the GA01 section, PFe distributions were predominantly controlled by lithogenic
350 material and to a smaller extent by remineralisation processes (as seen by a Factor 3 contribution of 4.1%). This
351 does not rule out some biogenic influences on PFe distribution, especially in [the surface](#), but this contribution is
352 ~~veiled-obscured~~ by the high lithogenic contribution. ~~The PMF analysis has been realised on the entire dataset, in~~
353 ~~consequence, the factors described are highly influenced by the major variations of particulate element~~
354 ~~concentrations (usually at the interface, i.e. margin, seafloor, surface layer,...).~~

355 To further investigate the influence of crustal material on the distribution of PFe, it is instructive to examine the
356 distribution of the molar ratio of PFe/PAI, ~~and the resulting %PFe_{litho}~~ (see section 2.6 for definition of this
357 ~~parameter~~) along the section ~~as a way to assess the lithogenic inputs~~ (Lannuzel et al., 2014; Ohnemus and Lam,
358 2015; Planquette et al., 2009) (Figure 6) ~~along the section~~.

Formatted: English (United Kingdom)

Formatted: English (United Kingdom)

359 The PFe/PAI ratio can be used to estimate the proportion of lithogenic particles within the bulk particulate
360 material. A comparison with the Upper Continental Crust (UCC) ratio of Taylor and McLennan (1995), 0.21, was
361 used to calculate the lithogenic components of particles (PFe_{litho}) following Eq. (1):

$$362$$
$$363 \quad \%PFe_{litho} = 100 * \left(\frac{PAI}{PFe} \right)_{sample} * \left(\frac{PFe}{PAI} \right)_{UCC \text{ ratio}} \quad (1)$$
$$364$$

365 Then the non-lithogenic PFe is simply obtained using Eq. (2):

$$366$$
$$367 \quad \%PFe_{non_litho} = 100 - \%PFe_{litho} \quad (2)$$
$$368$$

369 Both the lithogenic and non-lithogenic fraction of PFe are estimated using the UCC ratio. Spatial and temporal
370 variation of the lithogenic components ratio may falsely influence the estimated fraction value. The PFe_{litho} and
371 PFe_{non-litho} proxies are interesting tools to evaluate the importance of lithogenic and non-lithogenic (either biogenic
372 or authigenic), but have to be used with consideration.

373 Overall, the estimated lithogenic contribution to PFe varies from 25% (station 60, 950 m) to 100% at stations
374 located within the Western European Basin. [Note that](#) 100% of estimated lithogenic PFe does ~~no~~t necessary mean
375 that biogenic particles are absent; they may just be masked by the [important load dominance](#) of lithogenic particles.
376 Important inter-basins variations are observed along the section (Figure 6). The IAP and WEB basins are linked
377 with high median values of the proxy %PFe_{litho}, 90%, ~~which is also reflected in the MW and NEADW PFe/PAI~~
378 ~~ratio which -that displays a value PFe/PAI close to the crustal one (Figure 7).~~ ~~ou 8 dans la nouvelle version??).~~

379 This could be linked to ~~a~~ the lateral advection of iron rich lithogenic particles sourced from the Iberian margin
380 and to atmospheric [particulates inputs](#) (Shelley et al., 2017). This point is discussed ~~with in~~ more detail in section
381 ~~4.32.14. Then, between the stations 26 and 29, the %PFe_{litho} proxy values dramatically decreased, and reached~~
382 ~~values underless than 55%; between the stations 26 and 29, to reach median %PFe_{litho} value under 55% in the~~
383 ~~Iceland, Irminger and the Labrador basins.~~ This feature is likely ~~be~~ associated ~~to~~ with the presence of the Sub-
384 Arctic Front, located between 49.5 and 51°N latitude and 23.5 and 22°W longitude (Zunino et al., 2017). Indeed,
385 this front which separates cold and fresh water of subpolar origin from warm and salty water of subtropical origin

386 was clearly identifiable at station 26 by the steep gradient of the isotherms and isohalines between station 26 and
387 29; salinity dropping from 35.34 psu to 35.01 psu (Figure 2). North of the Sub-Arctic Front, LSW and ISOW
388 display high PFe/PAI ratios, ranging from 0.36 to 0.44 mol mol⁻¹. These high ratios, compared to the crustal one,
389 could be associated with higher content proportions of PFe from biogenic origin, especially in the case of the
390 LSW.

392 4.23. Tracking the different inputs of particulate iron

393 4.23.1. Inputs at margins: Iberian, Greenland and Newfoundland

394 Inputs from continental shelves and margins have been demonstrated to support high productivity in shallow
395 coastal areas. Inputs of iron from continental margin sediments supporting the high productivity found in shallow
396 coastal regions have been demonstrated in the past (e.g. Cullen et al. (2009), Elrod et al. (2004), Jeandel et al.
397 (2011), Ussher et al. (2007)) and sometimes, were shown to be advected at great distances from the coast (e.g.
398 Lam and Bishop et al., 2008).

399 In the following section, we will investigate these possible candidate sources in proximity of the different
400 margins encountered. Along the GEOVIDE section, sediments at margins were of various compositions
401 (Dutkiewicz et al., 2015). Sediments originating from the Iberian margin were mainly constituted of silts and clays
402 (Caeador et al., 1996; Duarte et al., 2014). East Greenland margin sediments were a mixture of sands and
403 grey/green muds, while, sediments from the West Greenland margin were mainly composed of grey/green muds
404 (Loring and Asmund, 1996). At the western end of the section, sediments from the Newfoundland margin were
405 composed of gravelly and sandy muds (Mudie et al., 1984). The different sediment compositions of the three
406 margins sampled during GEOVIDE have different mineralogy/composition, which are reflected in their different
407 PFe/PAI ratios (Figure 8). While the Iberian Margin had a PFe/PAI close to UCC ratio, the highest ratio could be
408 seen at the East Greenland (stations 53 and 56) and West Greenland (station 61) Margins, with median PFe/PAI
409 reaching 0.45 mol mol⁻¹. The Newfoundland margin displayed an intermediate behaviour, with Fe/Al ratios of
410 0.35 mol mol⁻¹.

411 In addition to PAI, PMn can be used as a tracer of inputs from shelf resuspension (Lam and Bishop, 2008). Indeed,
412 Mn is really sensitive to oxidation mediated by bacteria (Tebo et al., 1984; Tebo and Emerson, 1985) and forms
413 manganese oxides (MnO₂). These authigenic particles lead to an enrichment of Mn in particle compositions. In
414 order to track the influence of shelf resuspension, a percentage of sedimentary inputs “%bulk sediment inputs”
415 can be estimated using PMn/PAI ratio from GEOVIDE samples and the PMn/PAI UCC value (0.0034; Taylor and
416 McLennan, 1995) according to the following equation:

$$417 \quad \% \text{bulk sediment PMn} = 100 * \left(\frac{\text{PAI}}{\text{PMn}} \right)_{\text{sample}} + \left(\frac{\text{PMn}}{\text{PAI}} \right)_{\text{UCC ratio}} \quad (3)$$

418 This proxy is a good indicator of direct and recent sediment resuspension. We assume that particles newly
419 resuspended in water column will have the same PMn/PAI ratio than the UCC ratio leading to a “%bulk sediment
420 Mn” of 100%. This value will decrease by authigenic formation of Mn oxides. This proxy assumes homogeneity
421 of the sediment PMn/PAI ratio through the section which is maybe not completely the case at every station. In

422 consequence, this proxy is only a tool to identify new benthic resuspension at specific location and inter-
423 comparison between several locations is not possible. When a sample presents a “%bulk sediment Mn” greater
424 than 100%, we assign a value of 100% to simplify the following discussion. As the Mn cycle can also be affected
425 by biologic uptake (e.g. Peers and Price, 2004; Sunda and Huntsman, 1983), this proxy is only used at depths
426 where biologic activity is negligible (i.e. below 150m depth).

428 *The Iberian margin*

429
430 The Iberian margin was an important source of lithogenic-derived iron-rich particles ~~in~~ to the Atlantic Ocean
431 during GEOVIDE; shelf resuspension impacts ~~were~~ perceptible up to ~~at~~ 280 km ~~away~~ from the margin (Station
432 11) in the Iberian Abyssal Plain (Figure 8).

433 On the shelf, at station 2, high sediment resuspension ~~was observable by~~ resulted in the low beam transmissometry
434 value (87.6%) at the immediate vicinity of the seafloor (153 m). This sediment resuspension led to an extensive
435 input of lithogenic particles within the water column associated with high concentrations of PFe (304 nmol L⁻¹),
436 PAI (1500 nmol L⁻¹), and PMn (2.5 nmol L⁻¹) (Figure 3, Table S1). ~~Moreover, one hundred percent~~ 100% of PFe
437 ~~is~~ was estimated to have a lithogenic origin (Figure 10) while 100% of the PMn was estimated to be the result of
438 a recent sediment resuspension according to the %Fe_{litho} and “%bulk sediment Mn” proxies (supplementary
439 material, Table S2) (Figure 8), confirming the resuspended particle input.

440 Coastal waters of the Iberian Shelf are impacted by the runoff for the Tagus River, which is characterised by high
441 suspended matter discharges, ranging between 0.4 to 1 × 10⁶ tons yr⁻¹, and with a high anthropogenic signature
442 (Jouanneau et al., 1998). During the GEOVIDE section, the freshwater input was observable at stations 1, 2 and
443 4 in the first 20 m; salinity was below 35.2 psu while surrounding waters masses had salinity up to 35.7 psu.
444 Within the freshwater plume, particulate concentrations were important at station 2 with PFe of 1.83 nmol L⁻¹.
445 Further away from the coast, the particulate concentrations remained low at 20m depth, with PFe, PAI, and PMn
446 concentrations of 0.77 nmol L⁻¹, 3.5 nmol L⁻¹, and 0.04 nmol L⁻¹, respectively at station 1. The low expansion of
447 the Tagus plume is likely due to the rapid settling of suspended matter. Indeed, our coastal station 2 was already
448 located at around 50 km of the Iberian coast and according to Jouanneau et al. (1998), the surface particle load
449 can be observable at a maximum 30km of the Tagus estuary.

450 ~~In addition~~ Besides, ADCP data acquired during GEOVIDE (Zunino et al., 2017) and several other studies have
451 reported an intense current spreading northward coming from the Straits of Gibraltar and Mediterranean Sea,
452 leading to a the strong resuspension of benthic sediments above the Iberian Shelf, e.g. Biscaye and Eittrreim (1977),
453 Eittrreim et al. (1976), McCave and Hall (2002), Spinrad et al. (1983). The importance of the sediment
454 resuspension was observable by low beam transmissometry value (87.6%) at the bottom of station 2. This
455 important sediment resuspension led to an extensive input of lithogenic particles within the water column
456 associated with high concentrations of PFe (304 nmol L⁻¹), PAI (1500 nmol L⁻¹), and PMn (2.5 nmol L⁻¹) (Figure
457 3, Table S1).

458 ~~Moreover, one hundred percent of PFe is estimated to have a lithogenic origin (Figure 10) while 100% of the PMn~~
459 ~~was estimated to be the result of a recent sediment resuspension according to the %Fe_{litho} and “%bulk sediment~~
460 ~~Mn” proxies (supplementary material, Table S2), confirming the resuspended particle input.~~

Formatted: Space After: 10 pt

At distance from the shelf, within the Iberian Abyssal Plain, an important lateral advection of PFe from the margin was observable (Figure 498). These lateral inputs occurred at two depth ranges: between 400 and 1000 m as seen at stations 4 and 1, with PFe concentrations reaching 4 nmol L⁻¹, and between 2500 m and the bottom (3575 m) of station 1, with PFe concentrations reaching 3.5 nmol L⁻¹. While 100% of PFe had a lithogenic signature, the sedimentary source input estimation decreased, between 40% and 90% of the PMn (Figure 498). Transport of lithogenic particles was observable until station 11 (12.2°W) at 2500 m where PFe concentration was 7.74 nmol L⁻¹ and 60% of PMn had a sedimentary origin (Figure 49). It is noteworthy that, no particular increase in PFe, PMn or PAI was seen-observed between 500 and 2000 m depth, where the MOW spreads. This, which is consistent with the that was-observed DFe concentrations (Tonnard et al., this issue), yet in contrast with-to the-dissolved aluminium (DAL) concentrations-values (Menzel-Barraqueta et al, subm.2018, this issue) which were high in the MOW, and with the study of Ohnemus and Lam (2015) that reported a maximum PFe concentration at 695 m depth associated with the particle-rich Mediterranean Overflow Water (Eittrheim et al., 1976) in the IAP. However, their station was located further south of our station 1. The shallower inputs observed at stations 1 and 4 could therefore be attributed to sediment resuspension from the Iberian margin and nepheloid layer at depth for station 1.

Surface coastal waters of the Iberian Shelf are impacted by the runoff for the Tagus River, which is characterised by high suspended matter discharges, ranging between 0.4 to 1 × 10⁶ tons yr⁻¹, and with a high anthropogenic [trace element] signature (Jouanneau et al., 1998). During the GEOVIDE section, the freshwater input was observable at stations 1, 2 and 4 in the first 20 m; salinity was below 35.2 psu-while surrounding waters masses had salinity up to 35.7-psu. Within the freshwater plume, particulate concentrations were high at station 2 with PFe of 1.83 nmol L⁻¹. Further away from the coast, the particulate concentrations remained low at 20m depth, with PFe, PAI, and PMn concentrations of 0.77 nmol L⁻¹, 3.5 nmol L⁻¹, and 0.04 nmol L⁻¹, respectively at station 1. The low expansion of the Tagus plume is likely due to the rapid settling of suspended matter. Indeed, our coastal station 2 was already located at around approximately 50 km off from the Iberian coast, whereas the surface particle load can only be observed at a maximum distance of 30 km from the Tagus estuary-and-according-to (Jouanneau et al., 1998), the surface particle load can be observable at a maximum 30km of the Tagus estuary. Overall, the Iberian margin appears to be an important source of lithogenic-derived iron rich particles in the Atlantic Ocean. Therefore, the Iberian margin appears to be an important source of lithogenic-derived iron-rich particles in the Atlantic Ocean; shelf resuspension impact was perceptible until 280 km away from the margin (Station 11) in the Iberian Abyssal Plain.

South Greenland

Several studies already demonstrated the importance of icebergs and sea ice as source of dissolved and particulate iron (e.g. van der Merwe et al., 2011a, 2011b; Planquette et al., 2011; Raiswell et al., 2008). The Greenland shelf is highly affected by external fresh water inputs as ice melting or riverine runoff (Fragoso et al., 2016), that are important sources of iron to the Greenland Shelf (Bhatia et al., 2013; Hawkings et al., 2014; Statham et al., 2008). Along During GEOVIDE, the Greenland shelves were a source of particulate-rich meteoric water leading to a transfer of DFe to PFe by an-enhanced biological activity. Indeed,

500 ~~Both~~ East and West Greenland shelves (stations 53 and 60) had high concentration of particles (beam
501 transmissometry of 83%) and particulate trace elements, reaching 22.1 nmol L⁻¹ and 18.7 nmol L⁻¹ of PFe,
502 respectively (station 53 at 100m and station 61 at 136 m). Several studies have already demonstrated the
503 importance of icebergs and sea ice melting as sources of dissolved and particulate iron (e.g. van der Merwe et al.,
504 2011a, 2011b; Planquette et al., 2011; Raiswell et al., 2008). The Greenland shelf is highly affected~~influenced by~~
505 external fresh water inputs such as sea-ice-melting or riverine runoff (Fragoso et al., 2016), that~~which are~~
506 important sources of iron to the Greenland Shelf (Bhatia et al., 2013; Hawkings et al., 2014; Statham et al., 2008).
507 During the cruise, the relative freshwater observed (S_{<33} psu) within the first 25 meters of stations 53 and 61
508 ~~was~~ associated with high PFe (19 nmol L⁻¹), PAI (61 nmol L⁻¹), PMn (0.6 nmol L⁻¹) and a low beam
509 transmissometry (≤ 85%) (Figure 94 and Table S1). The associated p~~Particles associated~~ were enriched in iron
510 compared to aluminium, as PFe/PAI ratio was 0.3 within the meteoric water plume. High biological production,
511 in agreement with~~The high PP concentrations (reaching 197 nmol L⁻¹) resulting from high biological production,~~
512 induced by the supply of bioavailable dissolved iron from meteoric water (Raiswell et al., 2008; Statham et al.,
513 2008; Tonnard et al., submitted, this issue), led to a transfer of DFe to the particulate phase. This is in line with
514 the factfinding that around 30% PFe had a non-lithogenic origin. In addition, only 40% PMn originated from
515 resuspended sediments. Interestingly, these two proxies remained constant from the seafloor to the surface (Station
516 49, Figure 408), with around 25% of the PMn of sedimentary origin, which could be due to ~~an~~ important mixing
517 happening-occurring on the shelf. The lithogenic PFe could result from the release of PFe from Greenland bedrock
518 captured during the ice sheet formation on land.

519 The spatial extent of the off-shelf lateral transport of particles was not important on the east Greenland coast.
520 Indeed, no visible increase of particulate trace metal concentrations was visible at the first station off-shelf, station
521 60 (Figure 408), except at 1000 m depth, where a strong increase (up to 90%) of sedimentary PMn was seen. This
522 is probably due to the East Greenland Coastal Current (EGCC) that was located at station 53 whicc constrained
523 these inputs while stations 56 and 60 were under the influence of another strong current, the East Greenland-
524 Irminger current (EGIC) (Zunino et al., 2017).

525 To the west of the Greenland margin, lateral transport of particles was slightly more important. Noticeable
526 concentrations of particulate lithogenic elements were observable until station 64 located 125 km away from
527 shoreline. These particles had a decrease~~ing~~ PFe lithogenic contribution (50%) with a similar (25%) sedimentary
528 PMn content than closer to the margin. The increasing nature of non-lithogenic PFe is linked to the bloom in
529 surface waters (associated with a PFe/PAI ratio of 0.30 mol mol⁻¹, a PP of 197 nmol L⁻¹ at station 61 and a Chl-a
530 concentrations of 6.21 mg~~Chl-a concentration of 6.21 mg m⁻³ at station 61~~), with the gravitational settling of
531 biogenic PFe settling-down-along-the-transport-of-particles.

532 Therefore, particles newly resuspended from Greenland sediments are an important source, representing around
533 one~~a~~ third of the pMn pool, combined with surface inputs such as riverine runoff and/or ice-melting that are
534 delivering particles on the shelf, and also biological production. Unlike the Iberian shelf, the Greenland margin
535 was not an important provider of particulate metals inside the Irminger and Labrador Basins, due to the circulation
536 that constrained the extent of the margin plume.

537

538 ~~Therefore, particles newly resuspended from Greenland sediments are an important source, representing around~~
539 ~~a third of the pMn pool, combined with surface inputs such as riverine runoff and/or ice-melting that are delivering~~

540 ~~particles on the shelf and biological production. Unlike the Iberian shelf, Greenland margin was not an important~~
541 ~~provider of particulate metals inside the Irminger and Labrador Basin, due to the circulation that constrained the~~
542 ~~extent of the margin plume.~~

544 *The Newfoundland Shelf*

545 Previous studies [have](#) already described the influence of fresh water on the Newfoundland shelf from the Hudson
546 Strait and/or Canadian Arctic Archipelago (Fragoso et al., 2016; Yashayaev, 2007). Yashayaev (2007) also
547 monitored strong resuspension of sediments associated with the spreading of [the](#) Labrador Current along the West
548 Labrador margin.

549 Close to the Newfoundland coastline, at station 78, high fresh water discharge (≤ 32 psu) was observed in surface
550 [waters](#) (Benetti et al., 2017). Interestingly, these freshwater signatures were not associated with elevated
551 particulate trace metal concentrations. Distance of meteoric water sources implied a long travel time for the water
552 to spread through the Labrador Basin to our sampling stations. Along the journey, particles present originally may
553 have been removed from [the](#) water column by gravitational settling.

554 The proportion of lithogenic PFe was relatively high and constant ~~in the entire throughout the~~ water column, with
555 a median value of 70%. At station 78, 100% of the PMn had a sedimentary origin close to the seafloor (371 m).

556 The spreading of the recent sediment resuspension was observable until 140 m depth where the contribution of
557 sedimentary Mn was still 51% (Figure ~~408~~, Table S2). This could correspond to an intense nepheloid layer as
558 previously reported by Biscaye and Eittrheim (1977) (see also section 3.3.2). The high PFe concentration (184
559 nmol L^{-1} , station 78, 371 m) associated with a high percentage of sedimentary PMn (95%) observed at the bottom
560 of this station, was therefore the result of an important resuspension of shelf sediments. This was confirmed with
561 low transmissometry values of 95%.

562 The important phytoplanktonic community present (maximum Chl-a = 4.91 mg m^{-3} , Tonnard et al., in prep), is
563 linked to [a](#) low PFe ~~concentration~~ of 0.79 nmol L^{-1} at 10 m, but, with a high PFe/PAI ratio, up to 0.4, and PP
564 concentration of 97 nmol L^{-1} , confirming the biological [al](#) influence. Either the biogenic particles settled quickly,
565 and/or they were quickly remineralized. Concerning this latter process, intense remineralization at station 77 (7
566 $\text{mmol C m}^{-2} \text{ d}^{-1}$ compared to $4 \text{ mmol C m}^{-2} \text{ d}^{-1}$ in the Western European Basin) has been reported by Lemaitre et
567 al. (2018a and 2018b), which could explain the low PFe values throughout the water column.

568
569 ~~Along the GEOVIDE section, continental shelves provided an important load of particles within the surrounding~~
570 ~~water column. The three margins sampled during GEOVIDE behaved differently; the Iberian margin discharged~~
571 ~~high quantities of lithogenic particles far away from the coast while the Greenland and Newfoundland margins~~
572 ~~did not reveal important PFe concentrations. Spreading of particles is tightly linked to hydrodynamic conditions,~~
573 ~~which in the case of the Greenland margin, prevented long distance seeding of PFe. Moreover, each margin~~
574 ~~showed a specific PFe/PAI ratio (Figure 8) indicating different composition of the resuspended particles.~~
575 ~~Resuspended particles represent the composition of sediment at the margin if oxido-reductive transformation of~~
576 ~~iron and aluminium are considered negligible under these circumstances. Differences between margins were due~~
577 ~~to the presence of non-crystal particles, either biogenic or authigenic. Biological production in surface waters and~~
578 ~~authigenic formation of iron hydroxide produce particles with a higher PFe/PAI content and their export through~~

579 ~~the water column to the sediment increased the PFe/PAI ratio at depth. Regions where biological production is~~
580 ~~intense such as in the vicinity of Newfoundland presented higher PFe/PAI ratios of resuspended benthic particles.~~
581 Along the GEOVIDE section, continental shelves provided an important load of particles within the surrounding
582 water column. The three margins sampled during GEOVIDE behaved very differently; the Iberian margin
583 discharged high quantities of lithogenic particles far away from the coast while the Greenland and Newfoundland
584 margins did not reveal important PFe concentrations. Spreading of particles is tightly linked to hydrodynamic
585 conditions, which in the case of the Greenland margin, prevented long distance seeding of PFe. Moreover, each
586 margin showed a specific PFe/PAI ratio (Figure 98) indicating different composition of the resuspended particles.
587 Resuspended particles represent the composition of sediment at the margin if ~~oxido-reductive~~ redox transformation
588 of iron and aluminium are considered negligible under these circumstances. Differences between margins were
589 due to the presence of non-crustal particles, either biogenic or authigenic. Biological production in surface waters
590 and authigenic formation of iron hydroxide produced particles with a higher PFe/PAI content and their export
591 through the water column to the sediment increased the PFe/PAI ratio at depth. Regions where biological
592 production is intense such as in the vicinity of Newfoundland presented higher PFe/PAI ratios of resuspended
593 benthic particles.

594 595 4.23.2 Benthic resuspended sediments

596 Along the GEOVIDE section, Benthic nepheloid layers (BNLs) ~~BNLs are providing~~ high concentrations of
597 particulate trace elements to in the deep open ocean, contributing highly significantly to the total trace elements
598 budget of as iron. Along the GA01 section, BNLs were observable in each province, although they had different
599 intensities with different strengths (Figures 3 and 120).

600 Benthic nepheloid layers (BNLs) are important layers where local resuspension of sedimentary particles (Bishop
601 and Biscaye, 1982; Eittrheim et al., 1976; Rutgers Van Der Loeff et al., 2002) occur due to strong hydrographic
602 stresses (i.e. boundary currents, benthic storms and deep eddies) interacting with the ocean floor (Biscaye and
603 Eittrheim, 1977; Eittrheim et al., 1976; Gardner et al., 2017, 2018). Along the GA01 section, BNLs were observable
604 in each province with different strengths (Figures 3 and 12).

605 In BNLs located within the WEB, PFe concentrations reached up to 10 nmol L⁻¹ (stations 26 and 29, Table S1).
606 These concentrations were smaller than PFe concentrations encountered in BNL from the Icelandic (stations 32
607 and 34), Irminger (stations 42 and 44) and Labrador Basins (stations 68, 69 and 71), where benthic resuspension
608 led to PFe concentrations higher than 40 nmol L⁻¹, even reaching 89 nmol L⁻¹ at the bottom of station 71 (3736
609 m). Moreover, in the Irminger and Labrador Basins, PFe/PAI molar ratios within BNLs were higher than the ones
610 measured within the WEB at station 26 and 29. In the Irminger Basin, PFe/PAI reached 0.4 mol mol⁻¹ (Figure
611 10±), which could reveal a mixture of lithogenic and biogenic matter that had been previously exported. This
612 feature was also observed in the Labrador Basin, with PFe/PAI ratio ranging between 0.34 and 0.44 mol mol⁻¹. In
613 contrast, BNLs sampled in the WEB ~~have~~ clearly have a lithogenic imprint, with PFe/PAI molar ratios close to
614 the crustal one. Resuspended sediments with a non-crustal contribution seem to ~~hold~~ have a higher PFe contents
615 than sediments with ~~a~~ lithogenic characteristics. Nevertheless, interestingly all BNLs present during GEOVIDE
616 were spreading identically, with impacts observable up to 200 meters above the oceanic seafloor (Figure 10±), as
617 reflected in beam transmissometry values, and PFe concentrations, ~~which~~ that returned to ~~a~~ background levels at
618 200 m above the seafloor. The presence of these BNLs has also been reported by Le Roy et al. (submitted, this

619 issue) using radium-226 activity. Important differences of PFe intensities could also be due to different
620 hydrographic components and topographic characteristics. BNLs are occurring due to strong hydrographic
621 stresses (i.e. boundary currents, benthic storms and deep eddies) interacting with the ocean floor (Biscaye and
622 Eittrheim, 1977; Eittrheim et al., 1976; Gardner et al., 2017, 2018). They are. As previously explained, two main
623 triggers of BNLs are benthic storms and deep eddies; by definition, these processes are highly variable
624 geographically and temporally, but we have no physical data ~~could-whichwould~~ allow us to investigate further
625 this hypothesis further.

626 Benthic nepheloid layers (BNLs) are important layers where local resuspension of sedimentary particles (Bishop
627 and Biscaye, 1982; Eittrheim et al., 1976; Rutgers Van Der Loeff et al., 2002) occur due to strong hydrographic
628 stresses (i.e. boundary currents, benthic storms and deep eddies) interacting with the ocean floor (Biscaye and
629 Eittrheim, 1977; Eittrheim et al., 1976; Gardner et al., 2017, 2018). Along the GA01 section, BNLs were observable
630 in each province with different strengths (Figures 3 and 12).

631 Along the GEOVIDE section, BNLs are providing high concentrations of particulate trace element in the deep
632 open ocean, contributing highly to the total trace elements budget as iron.

633 634 4.2.3. Reykjanes Ridge inputs

635 Above the Reykjanes ridge, high PFe concentrations were determined/measured, reaching 16 nmol L⁻¹ just
636 above the seafloor, while increased DFe concentrations were reported to the East-east of the ridge (Tonnard et al.,
637 this issue). The exact sources of iron-rich particles cannot be well constrained, as they could come from active
638 hydrothermal vents or resuspension of particulate matter from new crustal matter produced at the ridge. According
639 to the oceanic circulation (Zunino et al., 2017; Garcia-Ibanez et al., 2017), hydrothermal particles could have been
640 seen in the ISOW within the Icelandic Basin. Nevertheless, at the vicinity of the ridge, scanning electron
641 microscope (SEM) analyses of our samples did reveal a number of biological debris and clays but not the presence
642 of iron (oxy-)hydroxide particles (supplementary figure S1), which are known to be highly produced close to
643 hydrothermal vents (Elderfield and Schultz, 1996). Their absence could thus indicate an absence of vents.
644 However, data from other proxies, such as helium-3, are-would be necessary to claim-confirm with more accuracy
645 the presence or absence of an hydrothermal source close to station 38.

646 647 4.3.2.4. Atmospheric inputs

648 Atmospheric deposition is an important input of trace elements in surface of the open ocean (e.g. Jickells et al.,
649 2005). Atmospheric inputs, both wet and dry, were reported to be low during the GEOVIDE cruise (Menzel-
650 Bbarraqueta et al., 2018, this issue; Shelley et al., 2017; 2018). In fact, oceanic particles measurements in surface
651 waters along the section did not reveal high PFe or PAI ~~e~~ concentrations, concentrations, therefore, the surface
652 composition of particles did not seem to be highly affected by atmospheric deposition at the time of the cruise.
653 One pattern is also interesting to note: the surface waters of the Iberian Abyssal Plain and Western European
654 Basin, between stations 11 and 23 presented a characteristic feature with really low PFe/PAI elemental ratios, of
655 0.11, smaller than the UCC ratio of 0.21 (Figure 6). Such low ratios have been reported in the same region by
656 Barrett et al. (2012). One possible explanation is given by Buck et al. (2010) who described Fe-depleted aerosols
657 in this area of the North Atlantic with PFe/PAI ratio below UCC ratio. However, Shelley et al. (2017) found a

658 higher PFe/PAI ratio around 0.25 is this area (their samples geoa5-6). This result, highlights some of the
659 difficulties ~~that in linking~~ atmospheric inputs to water column data (Baker et al., 2016), and implies a probable
660 fractionation after aerosol deposition. In addition, there is high spatial and temporal variability of atmospheric
661 deposition (Mahowald et al., 2005) and a certain degree of uncertainty about the dissolution processes of
662 atmospherically-transported particles (Bonnet and Guieu, 2004).

663
664

665 5. Conclusions

666

667 The investigation of the PFe compositions of suspended particulate matter along the GEOVIDE section in the
668 North Atlantic reflects the pervasive influence of crustal particles, augmented by sedimentary inputs at margins,
669 and within benthic nepheloid layers at depths. In consequence, variance of particulate iron along the section is
670 mainly explained by lithogenic factors.

671 Resuspension of sedimentary particles from continental shelves are responsible of high particulate iron
672 concentrations within the surrounding water column, and could be observed at long distances, in the case of the
673 Iberian margin. ~~Due to the hydrodynamics conditions, lithogenic particles are exported off shore up to 280 km
674 away off the Iberian margin.~~ Our results also demonstrate the impact of Arctic meteoric water ~~in the
675 biogeochemical cycle of trace elements~~ on the Greenland shelf, while in surface waters, the enhancement of
676 productivity by new bioavailable iron is leading to a transfer of dissolved iron to the particulate phase.

677 ~~Above the Reykjanes Ridge, resuspension of particles were responsible for the PFe enrichment of the Iceland
678 Scottish Overflow Water.~~

679 Our dataset allowed ~~ed~~ the investigation of scavenging processes that were sometimes visible at depths greater than
680 1000 m, these effects being the most pronounced within the WEB.

681 Overall, ~~PFe particulate iron~~ distributions in the North Atlantic ~~is are~~ strongly ~~affect~~ influenced by sources at its
682 boundaries (i.e. continental margins and seafloor). When combined with other datasets from the GEOTRACES
683 program in a modelling study, for example, use of ~~t~~ This work, within the frame of the GEOTRACES
684 program, data will ~~will~~ facilitate a ~~greater~~ better understanding of particulate iron ~~the cycle of cycling in the
685 particulate iron~~ North Atlantic, when combined to other datasets in a modelling exercise for example.

686

687 This investigation of the PFe compositions of suspended particulate matter along the GEOVIDE section in the
688 North Atlantic indicates ~~reflects~~ the pervasive influence of crustal particles, augmented by sedimentary inputs at
689 margins, and at depths, within benthic nepheloid layers. ~~Rare particles are responsible of high concentration In
690 particular, hallowed the export of~~ while in surface, ~~twill il faudrait une phrase d'ouverture plutôt~~
691 Indeed, along the GEOVIDE section, continental shelves provided an important load of particles within the
692 surrounding water column, with PFe mostly residing in non biogenic particulate form. The Iberian margin
693 discharged high quantities of lithogenic particles originating from riverine inputs far away from the coast while
694 the Greenland margin did not reveal a long distance seeding of PFe, due to hydrodynamic conditions. Both
695 Greenland and Newfoundland margins PFe resuspended particles were under a strong biogenic influence that
696 were exported at depth. This resulted in different remineralisation fluxes among the different provinces.
697 Scavenging processes could also be visible at depths greater than 1000 m, these effects being the most pronounced

Formatted: Justified, Line spacing: 1.5 lines, No widow/orphan control, Don't adjust space between Latin and Asian text, Don't adjust space between Asian text and numbers

Formatted: Font: Times New Roman, English (United Kingdom)

Formatted: Font: Times New Roman, English (United Kingdom)

Formatted: Font: Times New Roman, English (United Kingdom)

Formatted: Font: Times New Roman, English (United Kingdom)

Formatted: Font: (Default) Helvetica, 11 pt, Font color: Auto

698 within the Labrador Basin.
699 Finally, resuspended sediments above the Reykjanes Ridge increased the PFe composition of the Iceland Scottish
700 Overflow Water. A similar feature occurs for the Labrador Sea Water, as it flows from the Irminger Basin to the
701 Western European Basin.

702
703
704

705 Acknowledgments

706 We are greatly indebted to the captain and crew of the N/O Pourquoi Pas? for their help during the GEOVIDE
707 mission and clean rosette deployment. We would like to give special thanks to Fabien Pérault and Emmanuel de
708 Saint Léger for their technical expertise, to Catherine Schmechtig for the GEOVIDE database management and
709 Greg Cutter for his guidance in setting up the new French clean sampling system. We also would like to thank
710 Reiner Schlitzer for the Ocean Data View software (ODV).

711 This work was supported by the French National Research Agency (ANR-13-BS06-0014, ANR-12-PDOC-0025-
712 01), the French National Centre for Scientific Research (CNRS-LEFE-CYBER), the LabexMER (ANR-10-
713 LABX-19), and Ifremer. It was supported for the logistic by DT-INSU and GENAVIR.

714

715 References

716

717 Aguilar-Islas, A. M., Rember, R., Nishino, S., Kikuchi, T. and Itoh, M.: Partitioning and lateral transport of iron
718 to the Canada Basin, *Polar Sci.*, 7(2), 82–99, doi:10.1016/j.polar.2012.11.001, 2013.

719 Baker, A. R., Adams, C., Bell, T. G., Jickells, T. D. and Ganzeveld, L.: Estimation of atmospheric nutrient inputs
720 to the Atlantic Ocean from 50°N to 50°S based on large-scale field sampling: Iron and other dust-associated
721 elements, *Global Biogeochem. Cycles*, 27(3), 755–767, doi:10.1002/gbc.20062, 2013.

722 Baker, A. R., Landing, W. M., Bucciarelli, E., Cheize, M., Fietz, S., Hayes, C. T., Kadko, D., Morton, P. L.,
723 Rogan, N., Sarthou, G., Shelley, R. U., Shi, Z., Shiller, A. and van Hulten, M. M. P.: Trace element and isotope
724 deposition across the air–sea interface: progress and research needs, *Philos. Trans. R. Soc. A Math. Phys. Eng.*
725 *Sci.*, 374(2081), 20160190, doi:10.1098/rsta.2016.0190, 2016.

726 Barrett, P. M., Resing, J. A., Buck, N. J., Buck, C. S., Landing, W. M. and Measures, C. I.: The trace element
727 composition of suspended particulate matter in the upper 1000m of the eastern North Atlantic Ocean: A16N, *Mar.*
728 *Chem.*, 142–144, 41–53, doi:10.1016/j.marchem.2012.07.006, 2012.

729 [Benetti, M., Reverdin, G., Lique, C., Yashayaev, I., Holliday, N. P., Tynan, E., Torres-Valdes, S., Lherminier, P.,](#)
730 [Tréguer, P., and Sarthou, G.: Composition of freshwater in the spring of 2014 on the southern Labrador shelf and](#)
731 [slope, *Journal of Geophysical Research: Oceans*, 122, 1102–1121, 10.1002/2016jc012244, 2017.](#)

732

733 Berger, C. J. M., Lippiatt, S. M., Lawrence, M. G. and Bruland, K. W.: Application of a chemical leach technique
734 for estimating labile particulate aluminum, iron, and manganese in the Columbia River plume and coastal waters
735 off Oregon and Washington, *J. Geophys. Res.*, 113, C00B01, doi:10.1029/2007JC004703, 2008.

736 Bergquist, B. A., Wu, J. and Boyle, E. A.: Variability in oceanic dissolved iron is dominated by the colloidal
737 fraction, *Geochim. Cosmochim. Acta*, 71(12), 2960–2974, doi:10.1016/j.gca.2007.03.013, 2007.

738 Bhatia, M. P., Kujawinski, E. B., Das, S. B., Breier, C. F., Henderson, P. B. and Charette, M. A.: Greenland
739 meltwater as a significant and potentially bioavailable source of iron to the ocean, *Nat. Geosci.*, 6(4), 274–278,
740 doi:10.1038/ngeo1746, 2013.

741 Biscaye, P. E. and Eitrem, S. L.: Suspended Particulate Loads and Transports in the Nepheloid Layer of the
742 Abyssal Atlantic Ocean, *Dev. Sedimentol.*, 23(C), 155–172, doi:10.1016/S0070-4571(08)70556-9, 1977.

743 Bishop, J. K. B. and Biscaye, P. E.: Chemical characterization of individual particles from the nepheloid layer in
744 the Atlantic Ocean, *Earth Planet. Sci. Lett.*, 58(2), 265–275, doi:10.1016/0012-821X(82)90199-6, 1982.

745 Bishop, J. K. B. and Fleisher, M. Q.: Particulate manganese dynamics in Gulf Stream warm-core rings and
746 surrounding waters of the N.W. Atlantic, *Geochim. Cosmochim. Acta*, 51(10), 2807–2825, doi:10.1016/0016-
747 7037(87)90160-8, 1987.

748 Bonnet, S. and Guieu C.: Dissolution of atmospheric iron in seawater, *Geophys. Res. Lett.*, 31(3), L03303,
749 doi:10.1029/2003GL018423, 2004.

750 Boyle, E. A., Bergquist, B. A., Kayser, R. A. and Mahowald, N.: Iron, manganese, and lead at Hawaii Ocean
751 Time-series station ALOHA: Temporal variability and an intermediate water hydrothermal plume, *Geochim.*
752 *Cosmochim. Acta*, 69(4), 933–952, doi:10.1016/j.gca.2004.07.034, 2005.

753 Buck, C. S., Landing, W. M., Resing, J. A. and Measures, C. I.: The solubility and deposition of aerosol Fe and
754 other trace elements in the North Atlantic Ocean: Observations from the A16N CLIVAR/CO2repeat hydrography
755 section, *Mar. Chem.*, 120(1–4), 57–70, doi:10.1016/j.marchem.2008.08.003, 2010.

756 ~~Cacador, I., Vale, C. and Catarino, F.: The influence of plants on concentration and fractionation of Zn, Pb, and~~
757 ~~Cu in salt marsh sediments (Tagus Estuary, Portugal), *J. Aquat. Ecosyst. Heal.*, 5(3), 193–198,~~
758 ~~doi:10.1007/BF00124106, 1996.~~
759 ~~Cheize, M., Planquette, H. F., Fitzsimmons, J. N., Pelletier, E., Sherrell, R. M.,~~
760 ~~Lambert, C., Bucciarelli, E., Sarthou, G., Le Goff, M., Liorzou, C., Chéron, S., Viollier, E., and Gayet, N.:~~
761 ~~Contribution of resuspended sedimentary particles to dissolved iron and manganese in the ocean: An experimental~~
~~study, *Chemical Geology*. doi: 10.1016/j.chemgeo.2018.10.003, 2018.~~

762 Collier, R. and Edmond, J.: The trace element geochemistry of marine biogenic particulate matter, *Prog.*
763 *Oceanogr.*, 13(2), 113–199, doi:10.1016/0079-6611(84)90008-9, 1984.

764 Cullen, J. T., Chong, M. and Ianson, D.: British columbia continental shelf as a source of dissolved iron to the
765 subarctic northeast Pacific Ocean, *Global Biogeochem. Cycles*, 23(4), 1–12, doi:10.1029/2008GB003326, 2009.

766 Cutter, G. A. and Bruland, K. W.: Rapid and noncontaminating sampling system for trace elements in global
767 ocean surveys, *Limnol. Oceanogr. Methods*, 10(JUNE), 425–436, doi:10.4319/lom.2012.10.425, 2012.

768 Dammshäuser, A., Wagener, T., Garbe-Schönberg, D. and Croot, P.: Particulate and dissolved aluminum and
769 titanium in the upper water column of the Atlantic Ocean, *Deep. Res. Part I Oceanogr. Res. Pap.*, 73, 127–139,
770 doi:10.1016/j.dsr.2012.12.002, 2013.

771 Dehairs, F., Jacquet, S., Savoye, N., Van Mooy, B. A. S., Buesseler, K. O., Bishop, J. K. B., Lamborg, C. H.,
772 Elskens, M., Baeyens, W., Boyd, P. W., Casciotti, K. L. and Monnin, C.: Barium in twilight zone suspended
773 matter as a potential proxy for particulate organic carbon remineralization: Results for the North Pacific, *Deep.
774 Res. Part II Top. Stud. Oceanogr.*, 55(14–15), 1673–1683, doi:10.1016/j.dsr2.2008.04.020, 2008.

775 ~~Duarte, B., Silva, G., Costa, J. L., Medeiros, J. P., Azeda, C., Sá, E., Metelo, I., Costa, M. J. and Caçador, I.:
776 Heavy metal distribution and partitioning in the vicinity of the discharge areas of Lisbon drainage basins (Tagus
777 Estuary, Portugal), *J. Sea Res.*, 93(February), 101–111, doi:10.1016/j.seares.2014.01.003, 2014.~~

778 Dutay, J. C., Tagliabue, A., Kriest, I. and van Hulst, M. M. P.: Modelling the role of marine particle on large
779 scale 231Pa, 230Th, Iron and Aluminium distributions, *Prog. Oceanogr.*, 133, 66–72,
780 doi:10.1016/j.pocean.2015.01.010, 2015.

781 ~~Dutkiewicz, A., Müller, R. D., O’Callaghan, S. and Jónasson, H.: Census of seafloor sediments in the world’s
782 ocean, *Geology*, 43(9), 795–798, doi:10.1130/G36883.1, 2015.~~

783 Eitrem, S., Thorndike, E. M. and Sullivan, L.: Turbidity distribution in the Atlantic Ocean, *Deep. Res. Oceanogr.
784 Abstr.*, 23(12), 1115–1127, doi:10.1016/0011-7471(76)90888-3, 1976.

785 Elderfield, H. and Schultz, A.: Mid-Ocean Ridge Hydrothermal Fluxes and the Chemical Composition of the
786 Ocean, *Annu. Rev. Earth Planet. Sci.*, 24(1), 191–224, doi:10.1146/annurev.earth.24.1.191, 1996.

787 Ellwood, M. J., Nodder, S. D., King, A. L., Hutchins, D. A., Wilhelm, S. W. and Boyd, P. W.: Pelagic iron cycling
788 during the subtropical spring bloom, east of New Zealand, *Mar. Chem.*, 160, 18–33,
789 doi:10.1016/j.marchem.2014.01.004, 2014.

790 Elrod, V. A., Berelson, W. M., Coale, K. H. and Johnson, K. S.: The flux of iron from continental shelf sediments:
791 A missing source for global budgets, *Geophys. Res. Lett.*, 31(12), 2–5, doi:10.1029/2004GL020216, 2004.

792 Fitzwater, S. E., Johnson, K. S., Gordon, R. M., Coale, K. H. and Smith, W. O.: Trace metal concentrations in
793 the Ross Sea and their relationship with nutrients and phytoplankton growth, *Deep. Res. Part II Top. Stud.
794 Oceanogr.*, 47(15–16), 3159–3179, doi:10.1016/S0967-0645(00)00063-1, 2000.

795 Fragoso, G. M., Poulton, A. J., Yashayaev, I. M., Head, E. J. H., Stinchcombe, M. C. and Purdie, D. A.:
796 Biogeographical patterns and environmental controls of phytoplankton communities from contrasting
797 hydrographical zones of the Labrador Sea, *Prog. Oceanogr.*, 141, 212–226, doi:10.1016/j.pocean.2015.12.007,
798 2016.

799 Frew, R. D., Hutchins, D. A., Nodder, S., Sanudo-Wilhelmy, S., Tovar-Sanchez, A., Leblanc, K., Hare, C. E. and
800 Boyd, P. W.: Particulate iron dynamics during FeCycle in subantarctic waters southeast of New Zealand, *Global*
801 *Biogeochem. Cycles*, 20(1), 1–15, doi:10.1029/2005GB002558, 2006.

802 García-Ibáñez, M. I., Pardo, P. C., Carracedo, L. I., Mercier, H., Lherminier, P., Ríos, A. F. and Pérez, F. F.:
803 Structure, transports and transformations of the water masses in the Atlantic Subpolar Gyre, *Prog. Oceanogr.*, 135,
804 18–36, doi:10.1016/j.pocean.2015.03.009, 2015.

805 Gardner, W. D., Tucholke, B. E., Richardson, M. J. and Biscaye, P. E.: Benthic storms, nepheloid layers, and
806 linkage with upper ocean dynamics in the western North Atlantic, *Mar. Geol.*, 385, 304–327,
807 doi:10.1016/j.margeo.2016.12.012, 2017.

808 Gardner, W. D., Richardson, M. J. and Mishonov, A. V.: Global assessment of benthic nepheloid layers and
809 linkage with upper ocean dynamics, *Earth Planet. Sci. Lett.*, 482, 126–134, doi:10.1016/j.epsl.2017.11.008, 2018.

810 Gerringa, L. J. A., Rijkenberg, M. J. A., Schoemann, V., Laan, P. and de Baar, H. J. W.: Organic complexation
811 of iron in the West Atlantic Ocean, *Mar. Chem.*, 177, 434–446, doi:10.1016/j.marchem.2015.04.007, 2015.

812 Hawkings, J. R., Wadham, J. L., Tranter, M., Raiswell, R., Benning, L. G., Statham, P. J., Tedstone, A., Nienow,
813 P., Lee, K. and Telling, J.: Ice sheets as a significant source of highly reactive nanoparticulate iron to the oceans,
814 *Nat. Commun.*, 5(May), 1–8, doi:10.1038/ncomms4929, 2014.

815 Hwang, J., Druffel, E. R. M. and Eglinton, T. I.: Widespread influence of resuspended sediments on oceanic
816 particulate organic carbon: Insights from radiocarbon and aluminum contents in sinking particles, *Global*
817 *Biogeochem. Cycles*, 24(4), 1–10, doi:10.1029/2010GB003802, 2010.

818 Jeandel, C. and Oelkers, E. H.: The influence of terrigenous particulate material dissolution on ocean chemistry
819 and global element cycles, *Chem. Geol.*, 395, 50–66, doi:10.1016/j.chemgeo.2014.12.001, 2015.

820 Jeandel, C., Peucker-Ehrenbrink, B., Jones, M. T., Pearce, C. R., Oelkers, E. H., Godderis, Y., Lacan, F., Aumont,
821 O. and Arsouze, T.: Ocean margins: The missing term in oceanic element budgets?, *Eos, Transactions American*
822 *Geophysical Union*, 92(26), 217–224, doi: 10.1029/2011EO260001, 2011.

823 Jickells, T. D., An, Z. S., Andersen, K. K., Baker, A. R., Bergametti, C., Brooks, N., Cao, J. J., Boyd, P. W., Duce,
824 R. A., Hunter, K. A., Kawahata, H., Kubilay, N., LaRoche, J., Liss, P. S., Mahowald, N., Prospero, J. M., Ridgwell,
825 A. J., Tegen, I. and Torres, R.: Global iron connections between desert dust, ocean biogeochemistry, and climate,
826 *Science* (80-.), 308(5718), 67–71, doi:10.1126/science.1105959, 2005.

827 Jouanneau, J. M., Garcia, C., Oliveira, A., Rodrigues, A., Dias, J. A. and Weber, O.: Dispersal and deposition of
828 suspended sediment on the shelf off the Tagus and Sado estuaries, S.W. Portugal, *Prog. Oceanogr.*, 42(1–4), 233–
829 257, doi:10.1016/S0079-6611(98)00036-6, 1998.

830 Labatut, M., Lacan, F., Pradoux, C., Chmeleff, J., Radic, A., Murray, J. W., Poitrasson, F., Johansen, A. M., Thil,
831 F., Lacan, F., Pradoux, C., Chmeleff, J., Radic, A., Murray, J. W., Poitrasson, F., Johansen, A. M. and Thil, F.:

832 Iron sources and dissolved - particulate interactions in the seawater of the Western Equatorial Pacific, iron isotope
833 perspectives., ~~Global Biogeochem Cycles~~~~Global Biogeochemical Cycles~~, 1044–1065,
834 doi:10.1002/2014GB004928, 2014.

835 Lam, P. J. and Bishop, J. K. B.: The continental margin is a key source of iron to the HNLC North Pacific Ocean,
836 *Geophys. Res. Lett.*, 35(7), 1–5, doi:10.1029/2008GL033294, 2008.

837 Lam, P. J., Ohnemus, D. C. and Marcus, M. A.: The speciation of marine particulate iron adjacent to active and
838 passive continental margins, *Geochim. Cosmochim. Acta*, 80, 108–124, doi:10.1016/j.gca.2011.11.044, 2012.

839 Lam, P. J., Ohnemus, D. C. and Auro, M. E.: Size-fractionated major particle composition and concentrations
840 from the US GEOTRACES North Atlantic Zonal Transect, *Deep. Res. Part II Top. Stud. Oceanogr.*, 116, 303–
841 320, doi:10.1016/j.dsr2.2014.11.020, 2015.

842 Lam, P. J., Lee, J. M., Heller, M. I., Mehic, S., Xiang, Y. and Bates, N. R.: Size-fractionated distributions of
843 suspended particle concentration and major phase composition from the U.S. GEOTRACES Eastern Pacific Zonal
844 Transect (GP16), *Mar. Chem.*, (April), 0–1, doi:10.1016/j.marchem.2017.08.013, 2017.

845 Lannuzel, D., Bowie, A. R., van der Merwe, P. C., Townsend, A. T. and Schoemann, V.: Distribution of dissolved
846 and particulate metals in Antarctic sea ice, *Mar. Chem.*, 124(1–4), 134–146, doi:10.1016/j.marchem.2011.01.004,
847 2011.

848 Lannuzel, D., Van der Merwe, P. C., Townsend, A. T. and Bowie, A. R.: Size fractionation of iron, manganese
849 and aluminium in Antarctic fast ice reveals a lithogenic origin and low iron solubility, *Mar. Chem.*, 161, 47–56,
850 doi:10.1016/j.marchem.2014.02.006, 2014.

851 Lee, J. M., Heller, M. I. and Lam, P. J.: Size distribution of particulate trace elements in the U.S. GEOTRACES
852 Eastern Pacific Zonal Transect (GP16), *Mar. Chem.*, 201(September 2017), 108–123,
853 doi:10.1016/j.marchem.2017.09.006, 2017.

854 Lemaitre, N., planquette, H., Planchon, F., Sarthou, G., Jacquet, S., Garcia-Ibanez, M. I., Gourain, A., Cheize, M.,
855 Monin, L., Andre, L., Laha, P., Terryn, H., and Dehairs, F.: Particulate barium tracing significant mesopelagic
856 carbon remineralisation in the North Atlantic, *Biogeosciences Discussions*, doi:10.5194/bg-15-2289-2018, 2018a.

857 Lemaitre, N., Planchon, F., Planquette, H., Dehairs, F., Fonseca-Batista, D., Roukaerts, A., Deman, F., Tang, Y.,
858 Mariez, C., and Sarthou G.: High variability of export fluxes along the North Atlantic GEOTRACES section
859 GA01: Particulate organic carbon export deduced from the ²³⁴Th method, *Biogeosciences Discuss.*,
860 doi:10.5194/bg-2018-190, 2018b.

861 Le Roy, E., Sanial, V., Charette, M.A., Van Beek, P., Lacan, F., Jacquet, S.H., Henderson, P.B., Souhaut, M.,
862 García-Ibáñez, M.I., Jeandel, C. and Pérez, F.: The ²²⁶Ra-Ba relationship in the North Atlantic during
863 GEOTRACES-GA01, *Biogeosciences Discussions*, doi:10.5194/bg-2017-478, 2017.

864 ~~Loring, D. H. and Asmund, G.: Geochemical factors controlling accumulation of major and trace elements in~~
865 ~~Greenland coastal and fjord sediments, *Environ. Geol.*, 28(1), 2–11, doi:10.1007/s002540050072, 1996.~~

866 ~~Mahowald, N. M., Baker, A. R., Bergametti, G., Brooks, N., Duce, R. A., Jickells, T. D., Kubilay, N., Prospero,~~
867 ~~J. M. and Tegen, I.: Atmospheric global dust cycle and iron inputs to the ocean, *Global Biogeochem. Cycles*,~~
868 ~~19(4), doi:10.1029/2004GB002402, 2005.~~

869 Marsay, C. M., Lam, P. J., Heller, M. I., Lee, J. M. and John, S. G.: Distribution and isotopic signature of ligand-
870 leachable particulate iron along the GEOTRACES GP16 East Pacific Zonal Transect, *Mar. Chem.*, (November
871 2016), 1–14, doi:10.1016/j.marchem.2017.07.003, 2017.

872 Martin, J. H., Fitzwater, S. E., Michael Gordon, R., Hunter, C. N. and Tanner, S. J.: Iron, primary production and
873 carbon-nitrogen flux studies during the JGOFS North Atlantic bloom experiment, *Deep. Res. Part II*, 40(1–2),
874 115–134, doi:10.1016/0967-0645(93)90009-C, 1993.

875 McCave, I. N. and Hall, I. R.: Turbidity of waters over the Northwest Iberian continental margin, *Prog. Oceanogr.*,
876 52(2–4), 299–313, doi:10.1016/S0079-6611(02)00012-5, 2002.

877 Menzel Barraqueta, J.L., Schlosser, C., Planquette, H., Gourain, A., Cheize, M., Boutorh, J., Shelley, R., Pereira
878 Contreira, L., Gledhill, M., Hopwood, M.J. and Lherminier, P.: Aluminium in the North Atlantic Ocean and the
879 Labrador Sea (GEOTRACES GA01 section): roles of continental inputs and biogenic particle removal.
880 *Biogeosciences Discussions*, 1-28, doi: 10.5194/bg-2018-39, 2018.

881 Milne, A., Schlosser, C., Wake, B. D., Achterberg, E. P., Chance, R., Baker, A. R., Forryan, A. and Lohan, M.
882 C.: Particulate phases are key in controlling dissolved iron concentrations in the (sub)tropical North Atlantic,
883 *Geophys. Res. Lett.*, 44(5), 2377–2387, doi:10.1002/2016GL072314, 2017.

884 ~~Mudie, P. J., Keen, C. E., Hardy, I. A. and Vilks, G.: Multivariate analysis and quantitative paleoecology of~~
885 ~~benthic foraminifera in surface and Late Quaternary shelf sediments, northern Canada, *Mar. Micropaleontol.*,~~
886 ~~8(4), 283–313, doi:10.1016/0377-8398(84)90018-5, 1984.~~

887 Nuester, J., Shema, S., Vermont, A., Fields, D. M. and Twining, B. S.: The regeneration of highly bioavailable
888 iron by meso- and microzooplankton, *Limnol Oceanogr.*, 59(4), 1399–1409, doi:10.4319/lo.2014.59.4.1399,
889 2014.

890 Oelkers, E. H., Jones, M. T., Pearce, C. R., Jeandel, C., Eiriksdottir, E. S. and Gislason, S. R.: Riverine particulate
891 material dissolution in seawater and its implications for the global cycles of the elements, *Geosci.*, 344(11–12),
892 646–651, doi:10.1016/j.crite.2012.08.005, 2012.

893 Ohnemus, D. C. and Lam, P. J.: Cycling of lithogenic marine particles in the US GEOTRACES North Atlantic
894 transect, *Deep. Res. Part II Top. Stud. Oceanogr.*, 116, 283–302, doi:10.1016/j.dsr2.2014.11.019, 2015.

895 Peers, G. and Price, N. M.: A role for manganese in superoxide dismutases and growth of iron-deficient diatoms,
896 *Limnol. Oceanogr.*, 49(5), 1774–1783, doi:10.4319/lo.2004.49.5.1774, 2004.

Formatted: English (United Kingdom)

897 Planquette, H. and Sherrell, R. M.: Sampling for particulate trace element determination using water sampling
898 bottles: Methodology and comparison to in situ pumps, *Limnol. Oceanogr. Methods*, 10(5), 367–388,
899 doi:10.4319/lom.2012.10.367, 2012.

900 Planquette, H., Fones, G. R., Statham, P. J. and Morris, P. J.: Origin of iron and aluminium in large particles (>
901 53 µm) in the Crozet region, Southern Ocean, *Mar. Chem.*, 115(1–2), 31–42, doi:10.1016/j.marchem.2009.06.002,
902 2009.

903 Planquette, H., Sanders, R. R., Statham, P. J., Morris, P. J. and Fones, G. R.: Fluxes of particulate iron from the
904 upper ocean around the Crozet Islands: A naturally iron-fertilized environment in the Southern Ocean, *Global
905 Biogeochem. Cycles*, 25(2), doi:10.1029/2010GB003789, 2011.

906 Planquette, H., Sherrell, R. M., Stammerjohn, S. and Field, M. P.: Particulate iron delivery to the water column
907 of the Amundsen Sea, Antarctica, *Mar. Chem.*, 153, 15–30, doi:10.1016/j.marchem.2013.04.006, 2013.

908 Radic, A., Lacan, F. and Murray, J. W.: Iron isotopes in the seawater of the equatorial Pacific Ocean: New
909 constraints for the oceanic iron cycle, *Earth Planet. Sci. Lett.*, 306(1–2), 1–10, doi:10.1016/j.epsl.2011.03.015,
910 2011.

911 Raiswell, R., Benning, L. G., Tranter, M. and Tulaczyk, S.: Bioavailable iron in the Southern Ocean: The
912 significance of the iceberg conveyor belt, *Geochem. Trans.*, 9(1), 7, doi:10.1186/1467-4866-9-7, 2008.

913 Rijkenberg, M. J. A., Middag, R., Laan, P., Gerringa, L. J. A., Van Aken, H. M., Schoemann, V., De Jong, J. T.
914 M. and De Baar, H. J. W.: The distribution of dissolved iron in the West Atlantic Ocean, *PLoS One*, 9(6), 1–14,
915 doi:10.1371/journal.pone.0101323, 2014.

916 [Rutgers Van Der Loeff, M. M., Meyer, R., Rudels, B. and Raehor, E.: Resuspension and particle transport in the
917 benthic nepheloid layer in and near Fram Strait in relation to faunal abundances and ²³⁴Th depletion, *Deep. Res.-
918 Part I Oceanogr. Res. Pap.*, 49\(11\), 1941–1958, doi:10.1016/S0967-0637\(02\)00113-9, 2002.](#)

919 Sanders, R., Henson, S. A., Koski, M., De La Rocha, C. L., Painter, S. C., Poulton, A. J., Riley, J., Salihoglu, B.,
920 Visser, A., Yool, A., Bellerby, R. and Martin, A. P.: The Biological Carbon Pump in the North Atlantic, *Prog.
921 Oceanogr.*, 129(PB), 200–218, doi:10.1016/j.pocean.2014.05.005, 2014.

922 [Sarhou, G., Lherminier, and the GEOVIDE team: Introduction to the French GEOTRACES North Atlantic
923 Transect \(GA01\): GEOVIDE cruise, *Biogeosciences*, 15, 7097-7109, <https://doi.org/10.5194/bg-15-7097-2018>,
924 \[2018\]\(#\).](#)

925

926 Sarhou, G., Vincent, D., Christaki, U., Obernosterer, I., Timmermans, K. R. and Brussaard, C. P. D.: The fate of
927 biogenic iron during a phytoplankton bloom induced by natural fertilisation: Impact of copepod grazing, *Deep.
928 Res. Part II Top. Stud. Oceanogr.*, 55(5–7), 734–751, doi:10.1016/j.dsr2.2007.12.033, 2008.

929 Schlosser, C., Schmidt, K., Aquilina, A., Homoky, W. B., Castrillejo, M., Mills, R. A., Patey, M. D., Fielding, S.,
930 Atkinson, A. and Achterberg, E. P.: Mechanisms of dissolved and labile particulate iron supply to shelf waters
931 and phytoplankton blooms off South Georgia, Southern Ocean, *Biogeosciences Discuss.*, 0049(July), 1–49,
932 doi:10.5194/bg-2017-299, 2017.

933 Shelley, R. U., Landing, W. M., Ussher, S. J., Planquett, H. and Sarthou, G.: Characterisation of aerosol
934 provenance from the fractional solubility of Fe (Al, Ti, Mn, Co, Ni, Cu, Zn, Cd and Pb) in North Atlantic aerosols
935 (GEOTRACES GA01 and GA03), *Biogeosciences*, submitted(November), 1–31, doi:10.5194/bg-2017-415,
936 2017.

937 Shelley, R. U., Landing, W. M., Ussher, S. J., Planquette, H. and Sarthou, G.: Regional trends in the fractional
938 solubility of Fe and other metals from North Atlantic aerosols (GEOTRACES cruises GA01 and GA03) following
939 a two-stage leach, *Biogeosciences*, 155194(1), 2271–2288, doi:10.5194/bg-15-2271-2018, 2018.

940 Sherrell, R. M., Field, P. M. and Gao, Y.: Temporal variability of suspended mass and composition in the
941 Northeast Pacific water column: Relationships to sinking flux and lateral advection, *Deep. Res. Part II Top. Stud.*
942 *Oceanogr.*, 45(4–5), 733–761, doi:10.1016/S0967-0645(97)00100-8, 1998.

943 Spinrad, R. W., Zaneveld, J. R. and Kitchen, J.C.: A Study of the Optical Characteristics of the Suspended Particles
944 Benthic Nepheloid Layer of the Scotian Rise, *J. Geophys. Res.*, 88, 7641–7645, doi:10.1029/J088i03C03, 1983.

945 Statham, P. J., Skidmore, M. and Tranter, M.: Inputs of glacially derived dissolved and colloidal iron to the coastal
946 ocean and implications for primary productivity, *Global Biogeochem. Cycles*, 22(3), 1–11,
947 doi:10.1029/2007GB003106, 2008.

948 Straneo, F., Pickart, R. S. and Lavender, K.: Spreading of Labrador sea water: An advective-diffusive study based
949 on Lagrangian data, *Deep. Res. Part I Oceanogr. Res. Pap.*, 50(6), 701–719, doi:10.1016/S0967-0637(03)00057-
950 8, 2003.

951 Sunda, W. G. and Huntsman, S. A.: Effect of Competitive Interactions Between Manganese and Copper on
952 Cellular Manganese and Growth in Estuarine and Oceanic Species of the Diatom *Thalassiosira*, *Limnol.*
953 *Oceanogr.*, 28(5), 924–934, doi:10.4319/lo.1983.28.5.0924, 1983.

954 Tagliabue, A., Bopp, L., Dutay, J. C., Bowie, A. R., Chever, F., Jean-Baptiste, P., Bucciarelli, E., Lannuzel, D.,
955 Remenyi, T., Sarthou, G., Aumont, O., Gehlen, M. and Jeandel, C.: Hydrothermal contribution to the oceanic
956 dissolved iron inventory, *Nat. Geosci.*, 3(4), 252–256, doi:10.1038/ngeo818, 2010.

957 Tagliabue, A., Bowie, A. R., Boyd, P. W., Buck, K. N., Johnson, K. S. and Saito, M. A.: The integral role of iron
958 in ocean biogeochemistry, *Nature*, 543(7643), 51–59, doi:10.1038/nature21058, 2017.

959 Taylor, S. and McLennan, S.: The geochemical evolution of the continental crust, *Rev. Geophys.*, 33(2), 241–
960 265, doi:10.1029/95RG00262, 1995.

961 Tebo, B. M. and Emerson, S. R.: Effect of Oxygen Tension Manganese (II) Concentration and Temperature on
962 the Microbially Catalyzed Manganese-Ii Oxidation Rate in a Marine Fjord, *Appl. Environ. Microbiol.*, 50(5),
963 1268–1273, 1985.

964 Tebo, B. M., Nealsen, K. H., Emerson, S. and Jacobs, L.: Microbial mediation of Mn(II) and Co(II) precipitation
965 at the o₂/H₂S interfaces in two anoxic fjords, 29(6), 1247–1258, 1984.

966 Tonnard, M., Planquette, H., Bowie, A. R., van der Merwe, P., Gallinari, M., Desprez de Gésincourt, F., Germain,
967 Y., Gourain, A., Benetti, M., Reverdin, G., Tréguer, P., Boutorh, J., Cheize, M., Menzel Barraqueta, J., Pereira-
968 Contreira, L., Shelley, R., Lherminier, P., and Sarthou, G.: Dissolved iron in the North Atlantic Ocean and
969 Labrador Sea along the GEOVIDE section (GEOTRACES section GA01), *Biogeosciences Discuss.*,
970 <https://doi.org/10.5194/bg-2018-147>, 2018

971 Trefry, J. H., Trocine, R. P., Klinkhammer, G. P. and Rona, P. A.: Iron and copper enrichment of suspended
972 particles in dispersed hydrothermal plumes along the mid-~~???~~Atlantic Ridge, *Geophys. Res. Lett.*, 12(8), 506–
973 509, doi:10.1029/GL012i008p00506, 1985.

974 Ussher, S. J., Achterberg, E. P. and Worsfold, P. J.: Marine biogeochemistry of iron, *Environ. Chem.*, 1(2), 67–
975 80, doi:10.1071/EN04053, 2004.

976 Ussher, S. J., Worsfold, P. J., Achterberg, E. P., Laës, A., Blain, S., Laan, P., de Baar, H. J. W.: Distribution and
977 redox speciation of dissolved iron on the European continental margin, *Limnol. Oceanogr.*, 52(6), 2530–2539,
978 doi:10.4319/lo.2007.52.6.2530, 2007.

979 Van der Merwe, P., Lannuzel, D., Bowie, A. R., Mancuso Nichols, C. A. and Meiners, K. M.: Iron fractionation
980 in pack and fast ice in East Antarctica: Temporal decoupling between the release of dissolved and particulate iron
981 during spring melt, *Deep. Res. Part II Top. Stud. Oceanogr.*, 58(9–10), 1222–1236,
982 doi:10.1016/j.dsr2.2010.10.036, 2011a.

983 Van Der Merwe, P., Lannuzel, D., Bowie, A. R. and Meiners, K. M.: High temporal resolution observations of
984 spring fast ice melt and seawater iron enrichment in East Antarctica, *J. Geophys. Res. Biogeosciences*, 116(3), 1–
985 18, doi:10.1029/2010JG001628, 2011b.

986 Weinstein, S. E. and Moran, S. B.: Distribution of size-fractionated particulate trace metals collected by bottles
987 and in-situ pumps in the Gulf of Maine-Scotian Shelf and Labrador Sea, *Mar. Chem.*, 87(3–4), 121–135,
988 doi:10.1016/j.marchem.2004.02.004, 2004.

989 Yashayaev, I.: Hydrographic changes in the Labrador Sea, 1960-2005, *Prog. Oceanogr.*, 73(3–4), 242–276,
990 doi:10.1016/j.pocean.2007.04.015, 2007.

991 Yashayaev, I. and Loder, J. W.: Enhanced production of Labrador Sea Water in 2008, *Geophys. Res. Lett.*, 36(1),
992 doi:10.1029/2008GL036162, 2009.

993 Zunino, P., Lherminier, P., Mercier, H., Daniault, N., García-Ibáñez, M. I., and Pérez, F. F.: The GEOVIDE
994 cruise in May–June 2014 reveals an intense Meridional Overturning Circulation over a cold and fresh subpolar
995 North Atlantic. *Biogeosciences*, 14(23), 5323, 2017.

996

997

998

999

1000

1001

1002

1003

1004

1005

1006

1007

1008

1009

1010

1011

1012

1013

1014

1015

1016

1017

1018

1019

1020

1021

1022

1023

1024

1025

1026

1027

1028

1029

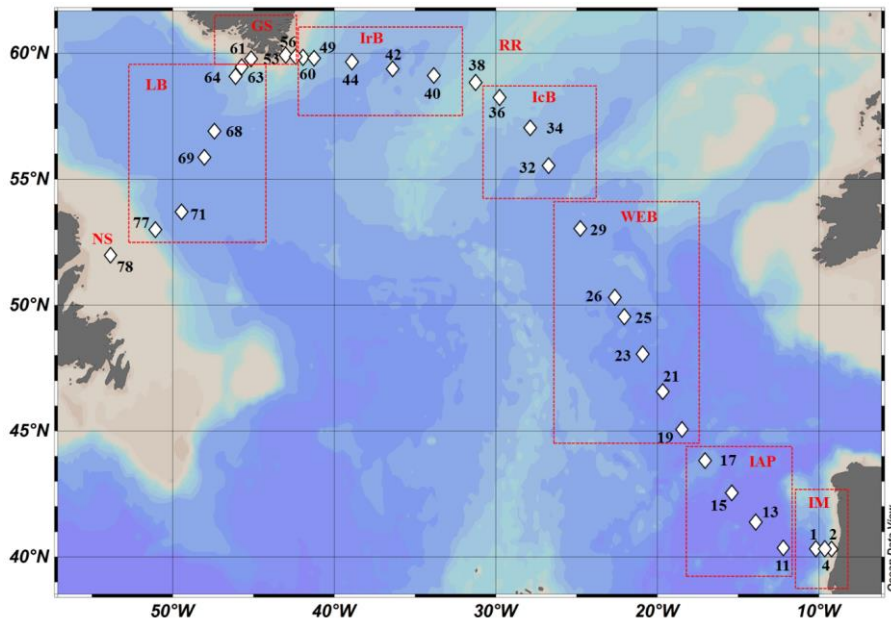
1030

1031

1032

1033
1034
1035
1036
1037
1038
1039
1040
1041
1042
1043
1044
1045

1046 Figure 1: Map of stations where suspended particle samples were collected with GO-FLO bottles during the GEOVIDE
1047 cruise (GA01). Biogeochemical provinces are indicated by red squares, IM: Iberian Margin, IAP: Iberian Abyssal
1048 Plain, WEB: Western European Basin, IcB: Iceland Basin, RR: Reykjanes Ridge, IrB: Irminger Basin, GS: Greenland
1049 Shelf, LB: Labrador Basin, NS: Newfoundland Shelf. This figure was generated by Ocean Data View (Schlitzer, R.,
1050 Ocean Data View, odv.awi.de, 2017).

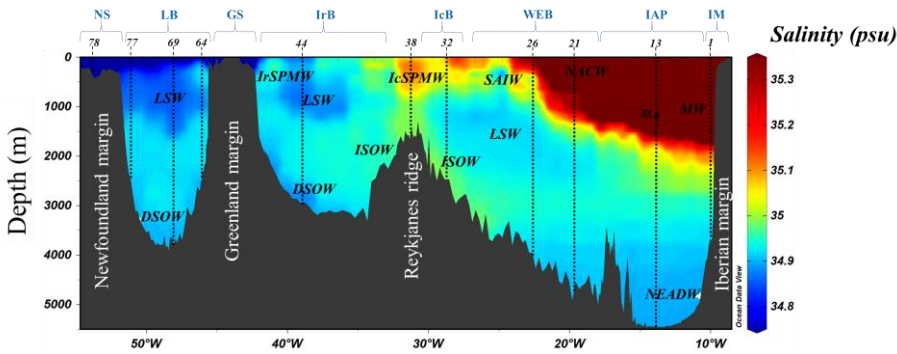


1051
1052
1053
1054
1055

1056
 1057
 1058
 1059
 1060
 1061
 1062
 1063
 1064
 1065
 1066
 1067
 1068
 1069
 1070
 1071
 1072
 1073

Figure 2: Salinity section during the GEOVIDE cruise. Water masses are indicated in black, MW: Mediterranean Water; NACW: North Atlantic Central Water; NEADW: North East Atlantic Deep Water; LSW: Labrador Sea Water; DSOW: Denmark Strait Overflow Water; ISOW: Iceland-Scotland Overflow Water; SAIW: Sub-Arctic Intermediate Water; IcSPMW: Iceland Sub-Polar Mode Water; IrSPMW: Irminger Sub-Polar Mode Water. Stations locations are indicated by the numbers. Biogeochemical provinces are indicated in blue font above station numbers. Contour of salinity = 35.8psu have been applied to identify the Mediterranean Water. This figure was generated by Ocean Data View (Schlitzer, R., Ocean Data View, odv.awi.de, 2017).

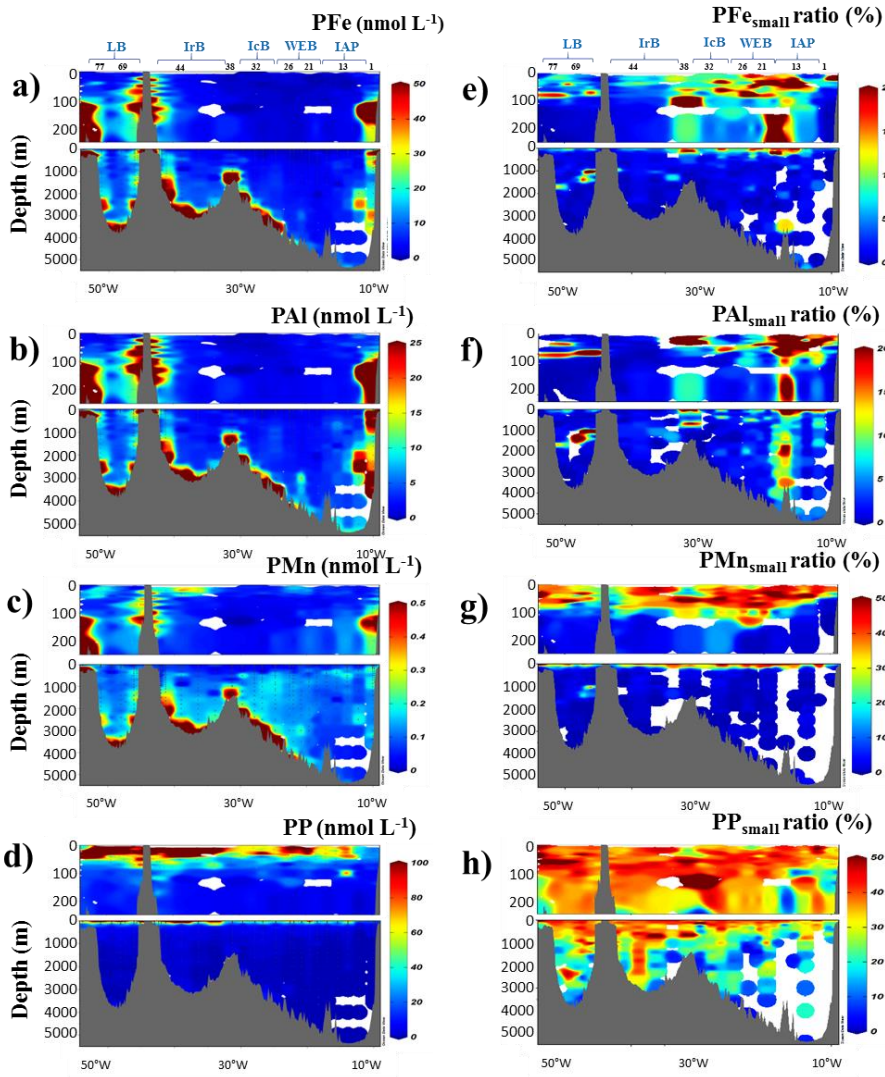
1074
 1075

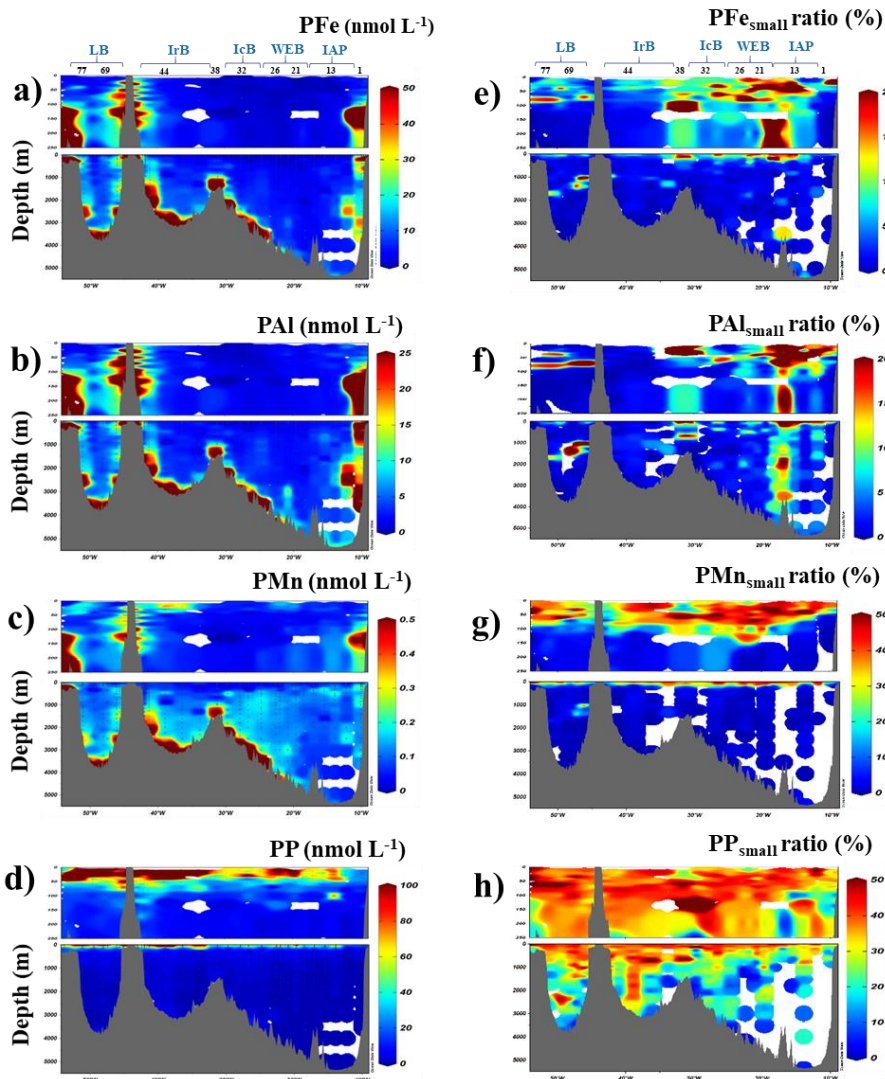


1076
 1077
 1078
 1079
 1080
 1081
 1082
 1083
 1084

1085
1086
1087
1088
1089
1090
1091
1092
1093
1094
1095

1096 Figure 3: Left panel: Distribution of (a) total particulate iron (a, PFe), (b) aluminium (b, PAL), (c) manganese (c, PMn)
1097 and (d) phosphorus (d, PP) concentrations (m-nmol L⁻¹) along the GEOVIDE section. Right panel: Contribution of
1098 the small size fraction (0,45-5 µm) expressed as a percentage (%) of the total concentration of (e) PFe (e), (f) PAL (f), (g)
1099 PMn (g) and (h) PP (h). Station IDs and biogeochemical regions are indicated on top of section a. This figure was
1100 generated by Ocean Data View (Schlitzer, R., Ocean Data View, odv.awi.de, 2017).





1102

1103

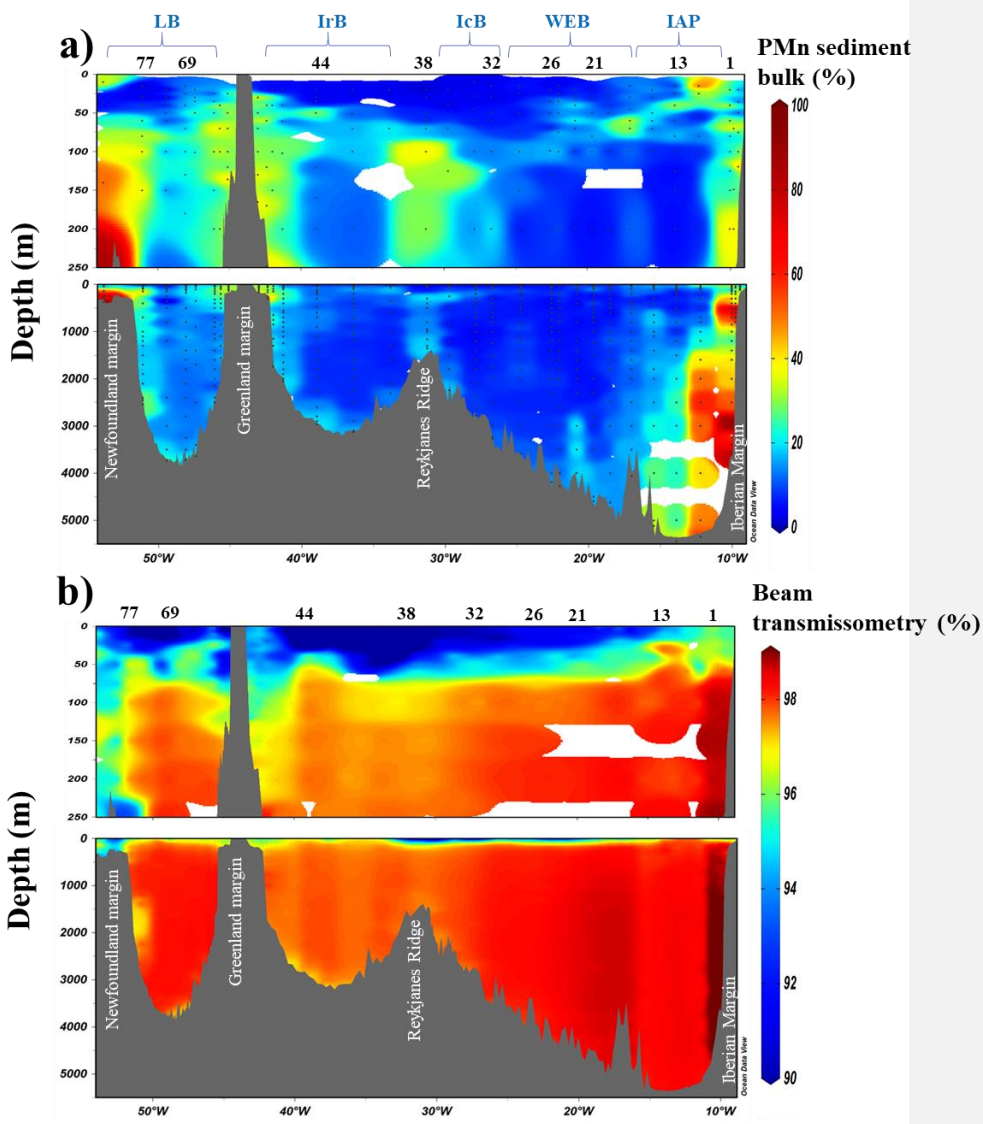
1104

1105

1106

1107

Figure 4: Section of derived contributions of sedimentary inputs (a) manganese bulk sediment proxy (a) and (b) transmissometry (b) along the GA01 section. Station IDs and biogeochemical region are indicated above the section (a). This figure was generated by Ocean Data View (Schlitzer, R., Ocean Data View, odv.awi.de, 2017).

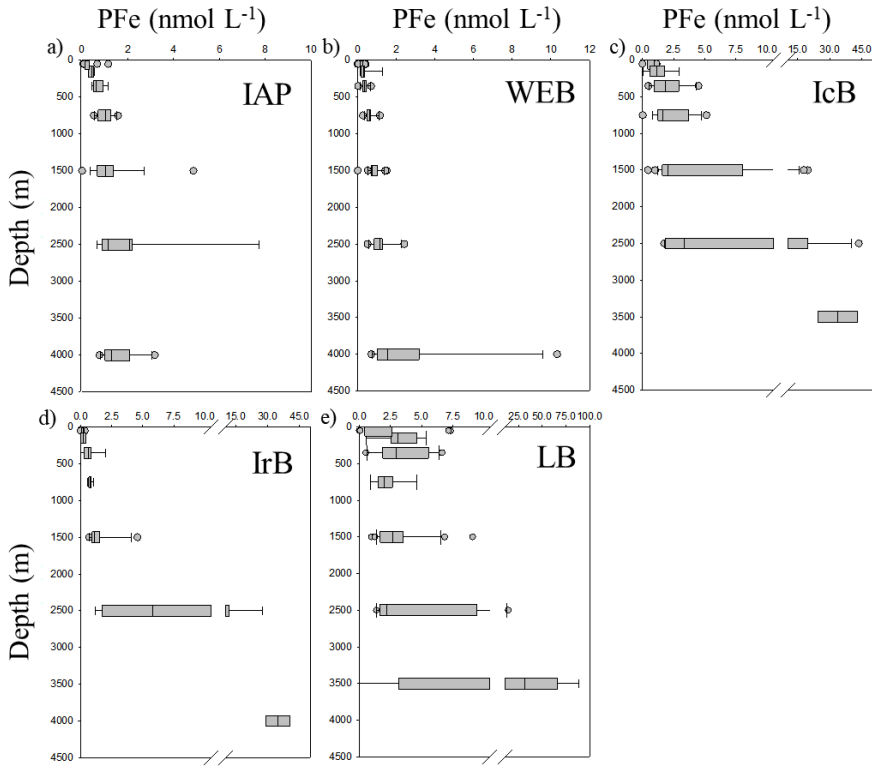


1108
1109
1110
1111

1112 **Figure 4: Boxplot figure of the particulate iron vertical profile (in nmol L^{-1}) in the a) Iberian abyssal plain (IAP), b)**
 1113 **Western European basin (WEB), c) Icelandic basin (IcB), d) Irminger basin (IrB) and e) Labrador basins (LB). Please**
 1114 **note the change of PFe scale between the basins. The left boundary of the box represents the 25th percentile while the**
 1115 **right boundary represents the 75th percentile, the line within the box marks the median value. Whiskers represent the**

1116
1117

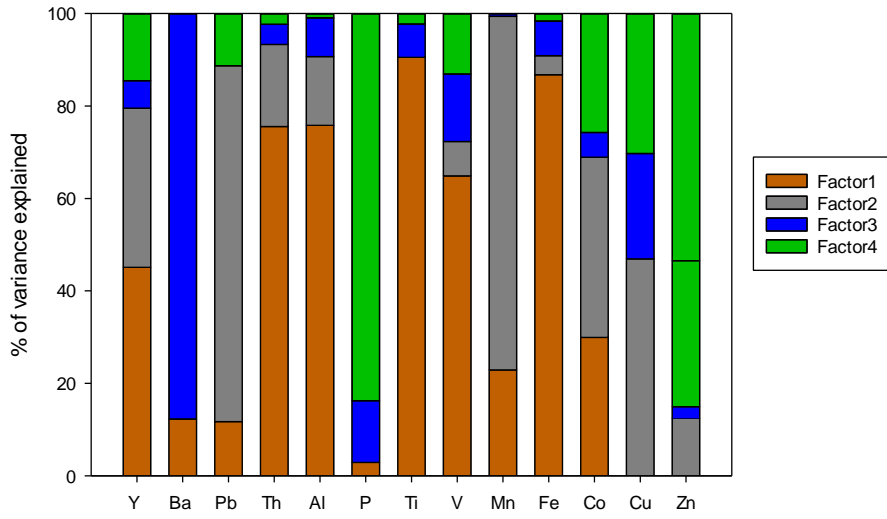
90th and 10th percentiles and dots are the outlying data. Seven depth-boxes have been used (0-100m, 100-200m, 200-500m, 500-1000m, 1000-2000m, 2000-3000m and 3000m-bottom depth).



1118
1119
1120
1121
1122
1123
1124
1125
1126
1127

1128 Figure 5: Factor fingerprint of the positive matrix factorisation. The four factors are represented in a stacked bar chart
1129 of the percentage of variance explained per element.

Commented [RS1]: It might be a good idea to list what each factor is dominated by, e.g. Factor 1 is dominated by the lithogenic elements, Ti, Fe, Al and Th, etc

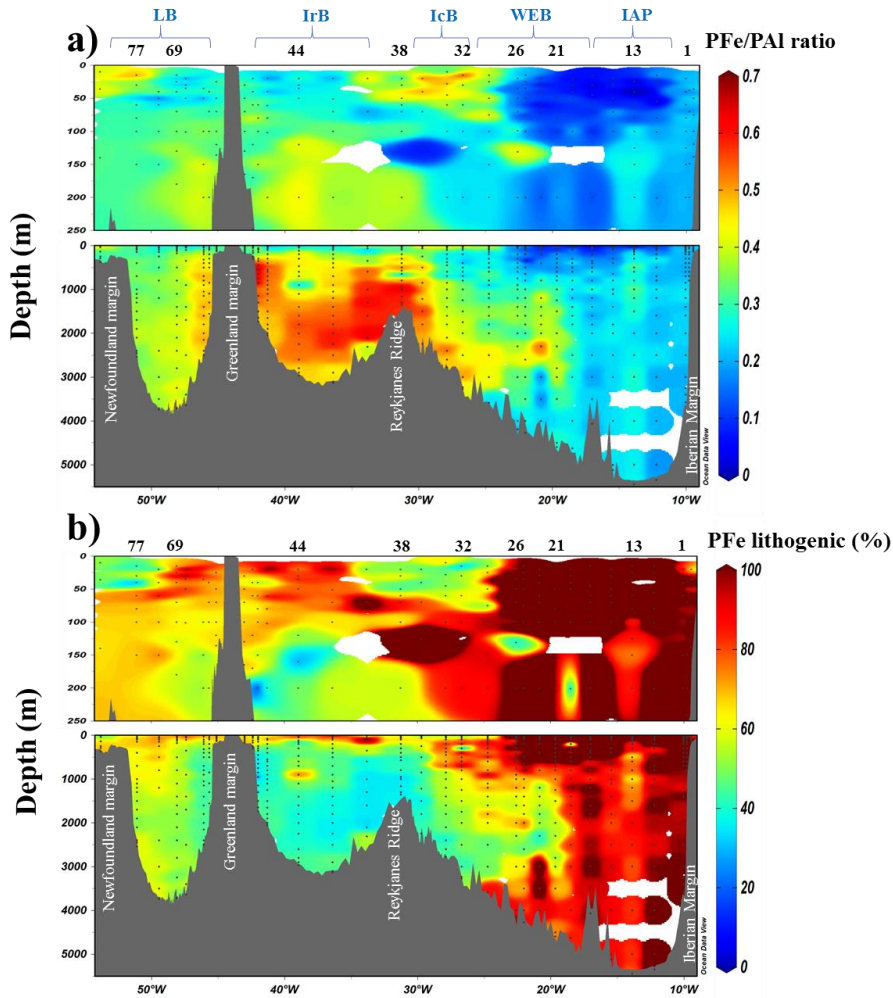


1130
 1131
 1132
 1133
 1134
 1135
 1136
 1137
 1138
 1139
 1140
 1141
 1142
 1143
 1144
 1145
 1146
 1147
 1148

1149
1150
1151

Figure 6: a) Section of the PFe to PAI molar ratio (mol mol^{-1}); (b) contribution of lithogenic PFe_{litho}(%) based on Eq. (1). Station IDs and biogeochemical provinces are indicated above each section. This figure was generated by Ocean Data View (Schlitzer, R., Ocean Data View, odv.awi.de, 2017).

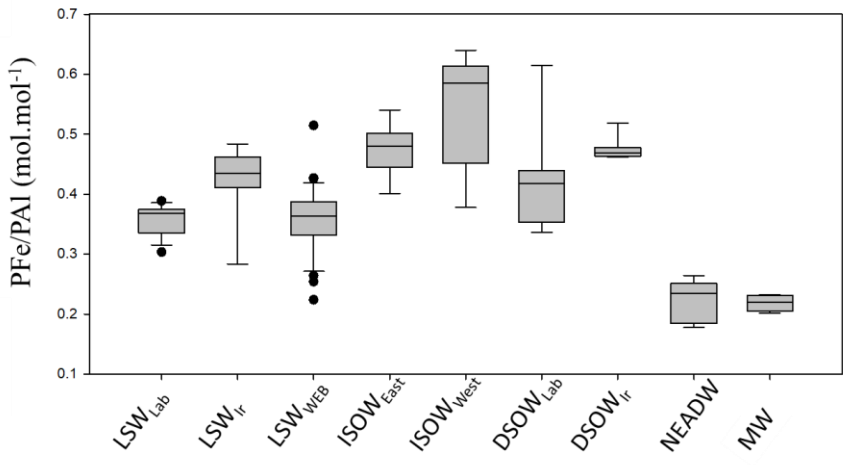
Formatted: Subscript



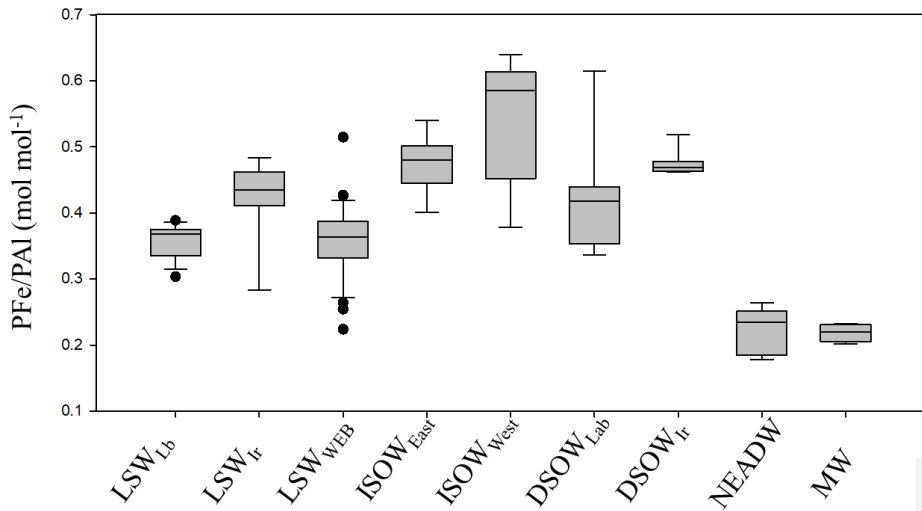
1152
1153
1154
1155
1156
1157
1158

1159 Figure 7: **Box and whisker diagram of PFe/PAI molar ratio (mol mol⁻¹)** in the different water masses sampled along
 1160 the GA01 line. Median values for the water masses were as follows: LSW_{lab}= 0.37; LSW_{lr}=0.44; LSW_{WEB}=0.36;
 1161 ISOW_{east}=0.48; ISOW_{west}=0.58; DSOW_{lab}=0.42; DSOW_{lr}=0.47; NEADW=0.23; MW=0.22 mol mol⁻¹. Based on their
 1162 salinity and potential temperature signatures (García-Ibáñez et al., 2015; Figure 2), we applied a Kruskal-Wallis test
 1163 onto the molar PFe/PAI ratios of nine water masses (Figure 7) in order to test the presence of significant differences.
 1164 Water masses for which we had less than 5 data points for PFe/PAI were excluded from this test. As the differences in
 1165 the median values among the treatment groups were greater than would be expected by chance; the difference in
 1166 PFe/PAI between water masses is statistically significant (P = <0.001).

Commented [RS2]: Probably don't need both of these as they are essentially saying the same thing



1167
1168

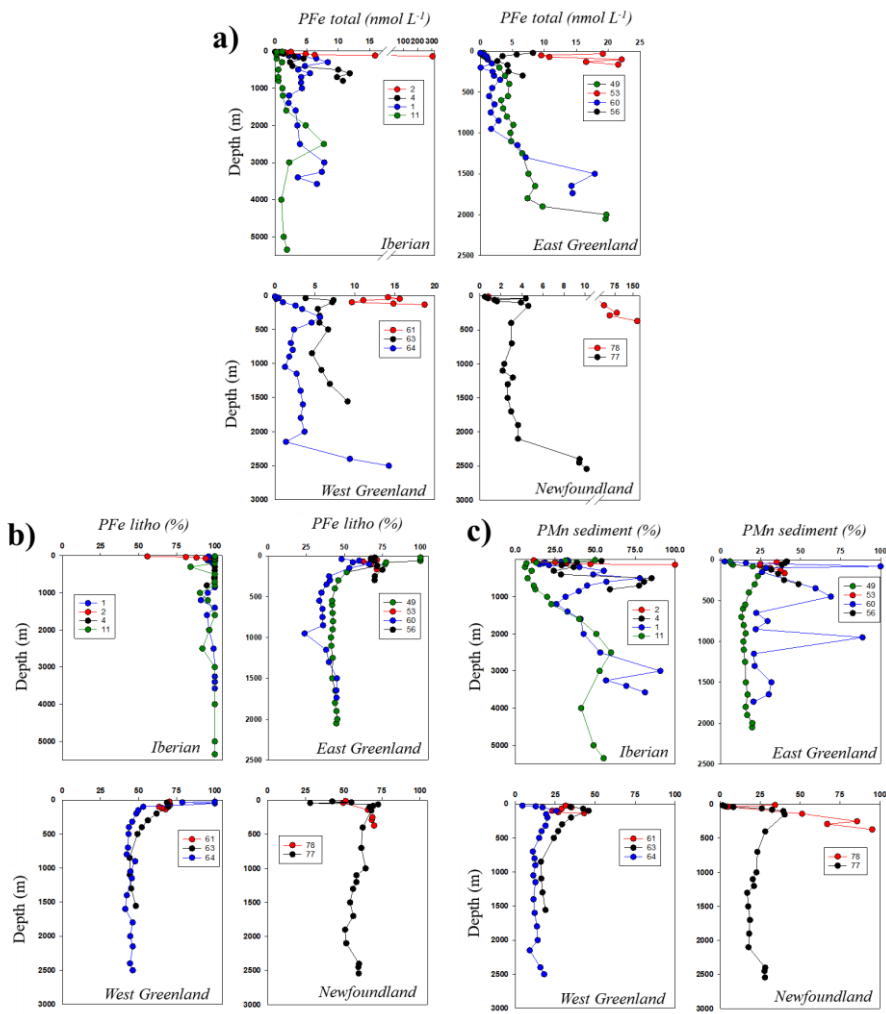


1169
1170

1171
1172
1173
1174
1175
1176
1177
1178
1179
1180
1181
1182

1183 Figure 8: Vertical profiles of (a) PFe (nmol L⁻¹), (b) lithogenic proportion of particulate iron (PFe_{litho}, %) and (c)
1184 sedimentary proportion of particulate manganese (PMn sediment, %) at the Iberian, East-West Greenland and
1185 Newfoundland margins.

Formatted: Subscript



1186

1187

1188

1189

1190

1191

1192

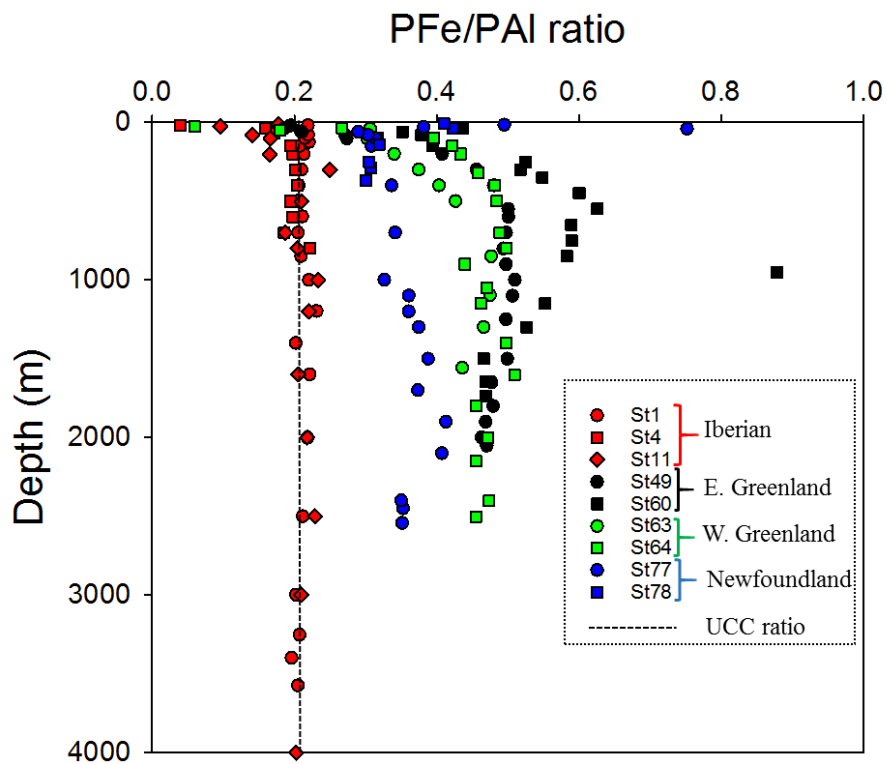
1193

1194

Formatted: Font: (Default) +Body (Calibri), 11 pt

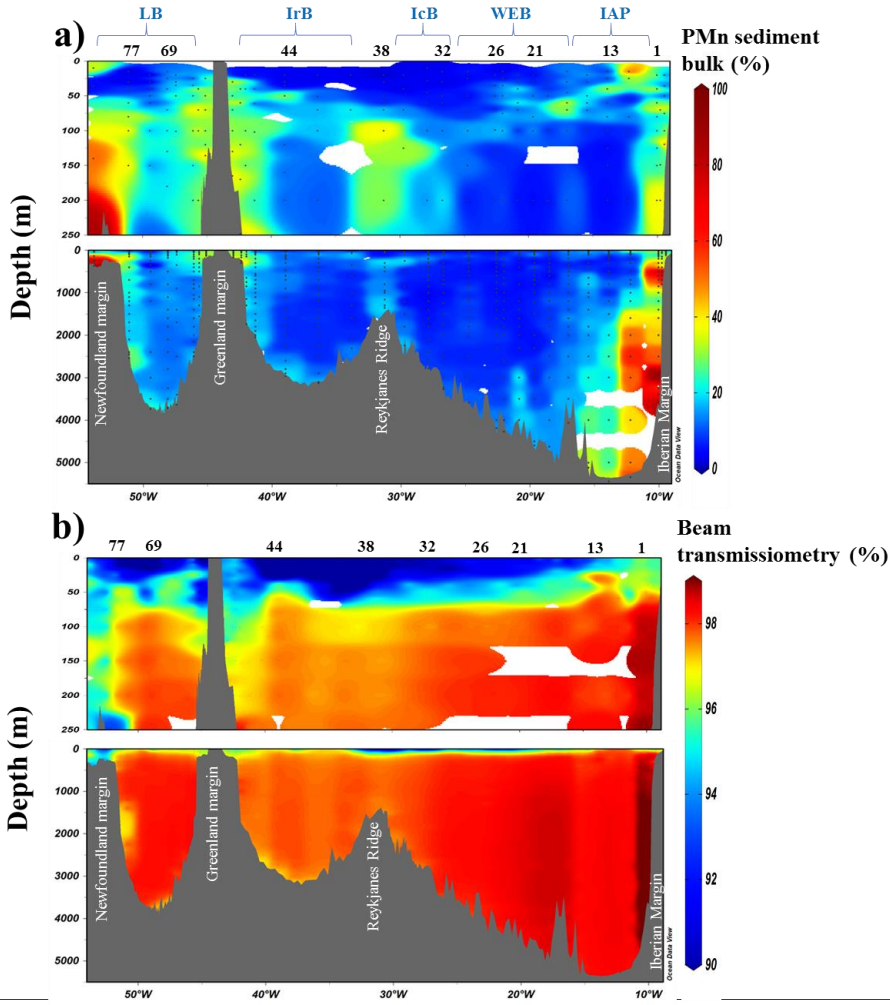
Formatted: Normal, Left

1195 Figure 89: Scatter of the PFe/PAI ratio at the Iberian (red dots), East Greenland (black dots), West Greenland (green
1196 dots) and Newfoundland margins (blue dots). Dashed line indicate the UCC ratio (Taylor and McLennan, 1995).



1197
1198
1199
1200
1201
1202
1203
1204
1205
1206
1207

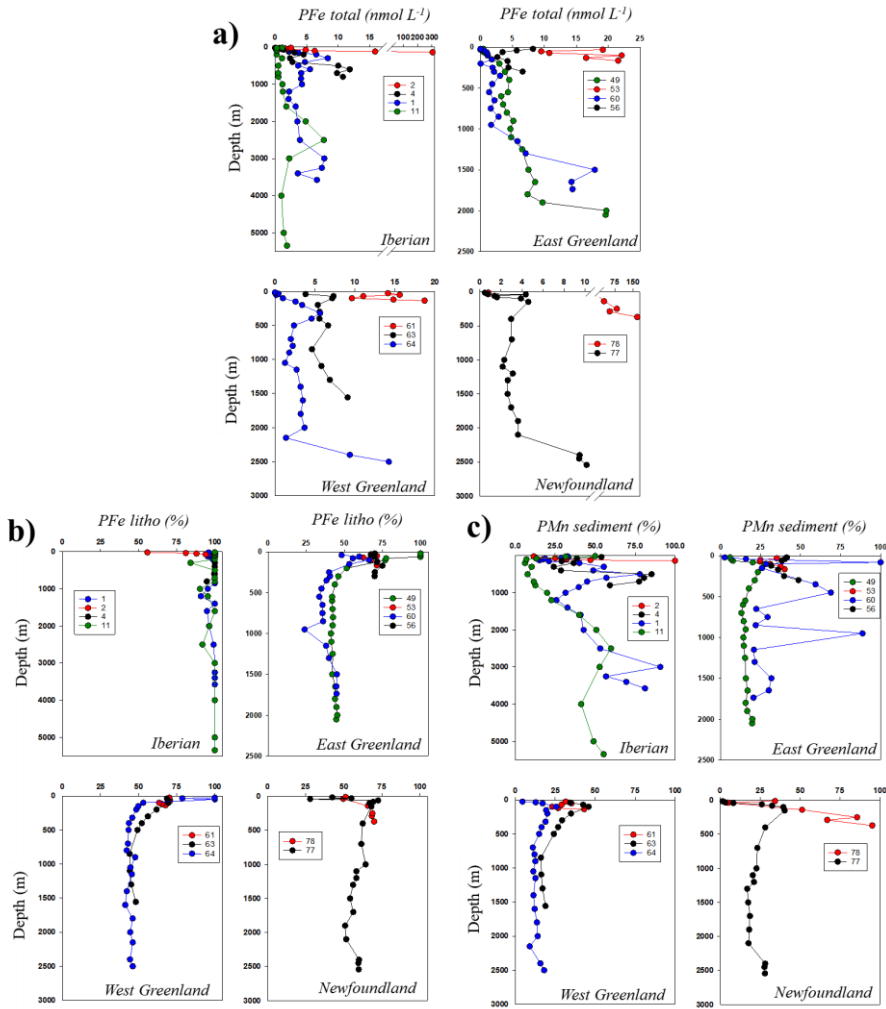
1208 **Figure 9: Section of derived contribution of sedimentary inputs manganese bulk sediment proxy (a) and**
 1209 **transmissiometry (b) along the GA01 section. Station IDs and biogeochemical region are indicated above the section (a).**
 1210 **This figure was generated by Ocean Data View (Schlitzer, R., Ocean Data View, odv.awi.de, 2017).**



1211
 1212
 1213
 1214
 1215
 1216

1217
1218

Figure 10: Vertical profiles of PFe (nmol L⁻¹, a), lithogenic proportion of particulate iron (%), b) and sedimentary proportion of particulate manganese (%), c) at the Iberian, East-West Greenland and Newfoundland margins.

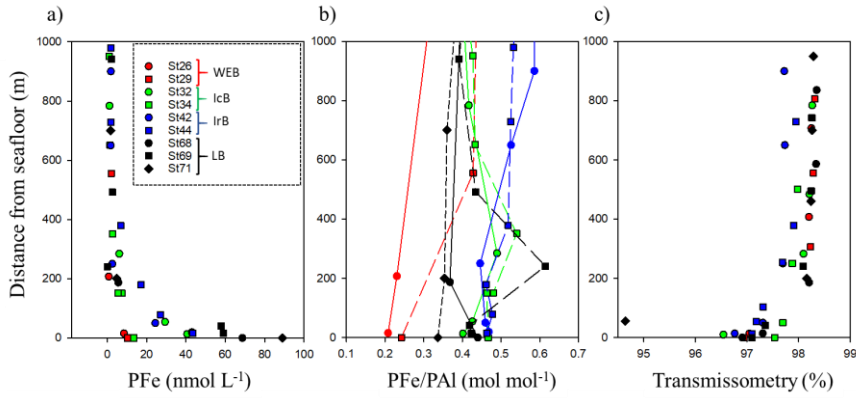


1219
1220
1221
1222
1223
1224
1225

1226
1227

Figure 140: PFe total (a); PFe/PAI ratio (b) and beam transmissometry (%) as a function of depth above the seafloor (m) at selected stations where a decrease in transmissometry was recorded.

Formatted: Font: Not Bold



1228
1229
1230
1231
1232
1233
1234
1235
1236
1237
1238
1239
1240
1241
1242
1243

		Fe	Al	P	Mn
Blank (nmol L ⁻¹)	5µm filter	0.072	0.100	0.511	0.003
	0.45µm filter	0.132	0.164	1.454	0.005
Limit of detection (nmol L ⁻¹)	5µm filter	0.011	0.030	0.365	0.001
	0.45µm filter	0.026	0.046	1.190	0.001
Recovery CRM (%)	BCR-414 (n=10)	88 ± 7			94 ± 7
	MESS-4 (n=5)	98 ± 14	97 ± 14	80 ± 30	110 ± 18
	PACS-3 (n=8)	101 ± 9	99 ± 14	91 ± 34	112 ± 11

1244

1245 **Table 1: Blank and limit of detection (nmol L⁻¹) of the two filters and Certified-certified reference material**
1246 **(CRM) recoveries during GEOVIDE suspended particle digestion.**

1247

1248

Author	Year	Fraction	Location	Depth range	PFe	PAI	PMn	PP
This study		>0.45µm	N. Atlantic (>40°N)	All	bdl-304	bdl-1544	bdl-3.5	bdl-402
Barrett et al.	2012	0.4µm	N. Atlantic (25-60°N)	Upper 1000m	0.29-1.71	0.2-19.7		
Dammshäuser et al.	2013	>0.2 µm	Eastern tropical N.A.	0-200		0.59-17.7		
Dammshäuser et al.	2013	>0.2 µm	Meridional Atlantic	0-200		0.35-16.1		
Lam et al.	2012	1-51 µm	Eastern tropical N.A.	0-600	ND-12			
Lannuzel et al.	2011	>0.2 µm	East Antarctic	Surface		0.02-10.67	0.01-0.14	
Lannuzel et al.	2014	>0.2 µm	East Antarctic	Fast ice	43-10385	121-31372	1-307	
Lee et al.	2017	>0.8 µm	Eastern tropical S.Pacific	All	bdl-159	bdl-162	bdl-8.7	bdl-983
Marsay et al.	2017	>0.4 µm	Ross Sea	All	0.68-57.3	ND-185	ND-1.4	5.4-404
Milne et al.	2017	>0.45µm	Sub-tropical N.A.	All	ND-140	ND-800		
Ohnemus et al.	2015	0.8-51 µm	N. Atlantic	All	0-938	0-3600		
Planquette et al.	2009	>53 µm	Southern Ocean	30-340	0.15-13.2	0.11-25.5		
Schlosser et al.	2017	>1 µm	South Georgia Shelf	All	0.87-267	0.6-195	0.01-3.85	
Sherrell et al.	1998	1-53µm	Northeast Pacific	0-3557		0.0-54.2		
Weinstein et al.	2004	>53 µm	Labrador Sea	0-250	0.1-1.2	0.1-1.5		
Weinstein et al.	2004	0.4-10µm	Labrador Sea	0-250	2.5	3.6	0.05	
Weinstein et al.	2004	>0.4 µm	Gulf of Maine	0-300	34.8	109		

1249

1250 **Table 2: Concentration (in nmol L⁻¹) of trace elements (PFe, PAI, PMn and PP) in suspended particles collected in**
1251 **diverse regions of the world's ocean. Bdl: below detection limit, ND: non-determined.**

1252

1253

1254